Institute of Geophysics
Polish Academy of Sciences

PUBLICATIONS
OF THE INSTITUTE OF GEOPHYSICS
POLISH ACADEMY OF SCIENCES

Geophysical Data Bases, Processing and Instrumentation

443 (E-13)

BOOK OF EXTENDED ABSTRACTS

International Symposium
on Drought and Climate Change,
24–25 November 2022

Warsaw 2022 (Issue 5)

INSTITUTE OF GEOPHYSICS
POLISH ACADEMY OF SCIENCES

PUBLICATIONS
OF THE INSTITUTE OF GEOPHYSICS
POLISH ACADEMY OF SCIENCES

Geophysical Data Bases, Processing and Instrumentation

443 (E-13)

BOOK OF EXTENDED ABSTRACTS

International Symposium
on Drought and Climate Change,
24–25 November 2022

Warsaw 2022

Published by the Institute of Geophysics, Polish Academy of Sciences

ISBN 978-83-66254-13-8 eISSN-2299-8020
DOI: 10.25171/InstGeoph_PAS_Publs-2022-028

Editorial Office
Instytut Geofizyki Polskiej Akademii Nauk
ul. Księcia Janusza 64, 01-452 Warszawa

C O N T E N T S

Publications of the Institute of Geophysics, Polish Academy of Sciences
Geophysical Data Bases, Processing and Instrumentation
vol. 443 (E-13), 2022, pp. 3–3
DOI: 10.25171/InstGeoph_PAS_Publs-2022-029
International Symposium on Drought and Climate Change, 24–25 November 2022

International Symposium on Drought and Climate Change

PREFACE

Jarosław J. NAPIÓRKOWSKI[1,✉] and Wen WANG[2,✉]

[1]Institute of Geophysics, Polish Academy of Sciences, Warszawa, Poland

[2]School of Resource and Environmental Engineering, Wuhan University of Technology, Wuhan, China

✉ j.napiorkowski@igf.edu.pl; wangwen@hhu.edu.cn

The International Symposium on Drought and Climate Change was organized within the framework of the NCN SHENG project HUMDROUGHT (humdrought.igf.edu.pl), by the Hohai University (China) and the Institute of Geophysics, Polish Academy of Sciences (Poland). The meeting was held online from 24–25 November 2022.

During the symposium, 4 Keynote and 19 standard Speeches were presented by representatives of 11 countries, namely: China, Columbia, Ethiopia, Germany, India, Iran, Italy, Netherlands, Poland, Spain, and Tunisia. The number of participants in the Symposium reached almost 50.

Drought-related issues have been discussed, focusing on multiple spatiotemporal scales to pin-point global to continental trends, as well as showing how drought affects specific countries and catchments.

The abstracts collected here touch on multiple topics and techniques, such as: i) drought change assessment, ii) drought propagation, iii) soil moisture and ecological drought, iv) drought monitoring and modelling, including the use of remote sensing, v) human effects on drought development and propagation, vi) drought prediction and uncertainty analysis.

Keywords: China, Drought, HUMDROUGHT, Poland.

Received 23 November 2022
Accepted 20 December 2022

Publications of the Institute of Geophysics, Polish Academy of Sciences
Geophysical Data Bases, Processing and Instrumentation
vol. 443 (E-13), 2022, pp. 5–5
DOI: 10.25171/InstGeoph_PAS_Publs-2022-030
International Symposium on Drought and Climate Change, 24–25 November 2022

From Meteorological to Hydrological Drought in Europe: Amplification and Recovery

Christian MASSARI

Research Institute for Geo-Hydrological Protection, National Research Council CNR, Perugia, Italy

✉ christian.massari@irpi.cnr.it

A b s t r a c t

Climate change will increase in frequency and intensity of period with below than normal precipitation. During such periods, known as meteorological droughts, the decline in annual run-off may be proportionally larger than the corresponding decline in precipitation. Reasons behind this exacerbation of runoff deficit during dry periods remain largely unknown, and this challenges the predictability of when this exacerbation will occur in the future and how intense it will be. In this presentation I will discuss the role played by evaporation and subsurface storage in the propagation of the meteorological drought as well as processes related to the amplification and recovery of such phenomena. Understanding this has important implications for defining sustainable water management strategies and understanding potential ecological traits and is becoming more and more urgent due to the increasing frequency and magnitude of drought events like the one that has hit Italy in 2022.

Keywords: climate change, Europe, hydrological drought, meteorological drought.

Received 17 November 2022
Accepted 20 December 2022

Publications of the Institute of Geophysics, Polish Academy of Sciences
Geophysical Data Bases, Processing and Instrumentation
vol. 443 (E-13), 2022, pp. 7–7
DOI: 10.25171/InstGeoph_PAS_Publs-2022-031
International Symposium on Drought and Climate Change, 24–25 November 2022

Flash Drought Propagation in the Yangtze River Basin under Climate Change

Liyan YANG, Weiguang WANG✉, and Jia WEI

Hohai University, China

✉ wangweiguang2016@126.com

Abstract

Flash drought is a space-time phenomenon with rapid intensification which poses serious threats to terrestrial ecosystems. However, the understand of flash drought propagation under climate change and regional human activities is still insufficient, and its potential causes remain unresolved. To explore this key issue, an integrated framework is proposed to describe the drought propagation process in the Yangtze River Basin, and trend and attribution analyses are utilized to explore potential influence factors. The framework is conducive to better understanding of flash drought processes and provides scientific guidance for flash drought early warning, prevention and mitigation.

Keywords: flash drought, drought propagation, Yangtze River Basin, climate change.

Received 17 November 2022
Accepted 20 December 2022

Publications of the Institute of Geophysics, Polish Academy of Sciences
Geophysical Data Bases, Processing and Instrumentation
vol. 443 (E-13), 2022, pp. 9–13
DOI: 10.25171/InstGeoph_PAS_Publs-2022-032
International Symposium on Drought and Climate Change, 24–25 November 2022

Remote Sensing as a Tool to Monitor Drought at the Watershed Scale

Ali Alperen İSCAN[1,✉] and Michael NONES[2]

[1]Brandenburgische Technische Universität Cottbus-Senftenberg, Cottbus, Germany

[2]Institute of Geophysics, Polish Academy of Sciences, Warszawa, Poland

✉ alperen.iscann@gmail.com

A b s t r a c t

Drought occurs due to the accumulative effect of certain climatological and hydrological variables over a certain period. As droughts are becoming a frequent phenomenon also in regions generally not affected by them, they are becoming a significant research topic, also thanks to the development of advanced monitoring methods and models. Focusing on the Vistula basin in Poland, the present work investigates changes in drought indexes and connected metrics by analysing satellite data. The use of satellite information allows for deriving trends at the watershed scale, therefore providing spatially-distributed medium/long-term changes. The present analysis takes advantage of the potentiality of Google Earth Engine and its freely-available datasets, showing that nowadays drought is a major concern also for a region that used to be wetter in the past.

Keywords: drought, Google Earth Engine, Poland, remote sensing.

1. INTRODUCTION

The observed increase in the frequency of droughts and heatwaves over the Northern Hemisphere in the 21st century poses socio-economic threats affecting the well-being of the people by triggering negative effects (Rakovec et al. 2022). These adverse hydro-meteorological conditions can lead to agricultural and ecological impacts, poor water quality conditions, wildfires even threatening existing infrastructure (Kreibich et al. 2022).

Like many other countries in Central Europe, also Poland recently faced more severe droughts, as depicted in the present study. To address changes at the sub-basin scale, drought indices are here computed using Google Earth Engine (GEE), an online cloud-based platform (Gorelick et al. 2017) that runs on python/java API and is largely used for manipulating and performing operations on image or image collections (Khan and Gilani 2021; Boothroyd et al. 2021). GEE has a massive catalogue of datasets available for users and allows for efficient algorithm development, processing of the datasets, and crowdsourcing (Xiong et al. 2017).

2. MATERIALS AND METHODS

2.1 Study area

The study focuses on the Vistula River basin, which has a total drainage basin area of 193,960 km^2, of which 87% (169,000 km^2) lies within Poland. The remaining part of the basin is located in Belarus, Ukraine, and Slovakia (Fig. 1). The land use structure is dominated by arable land (66%), while forests and semi-natural ecosystems cover 29%, and only 3% are classified as urban areas. The Polish climate is generally cold, without a dry season and with a warm summer. In the south, cold, no dry seasons, and cold summers are also present, while the highest mountains can show tundra-like characteristics (Karamuz and Romanowicz 2021).

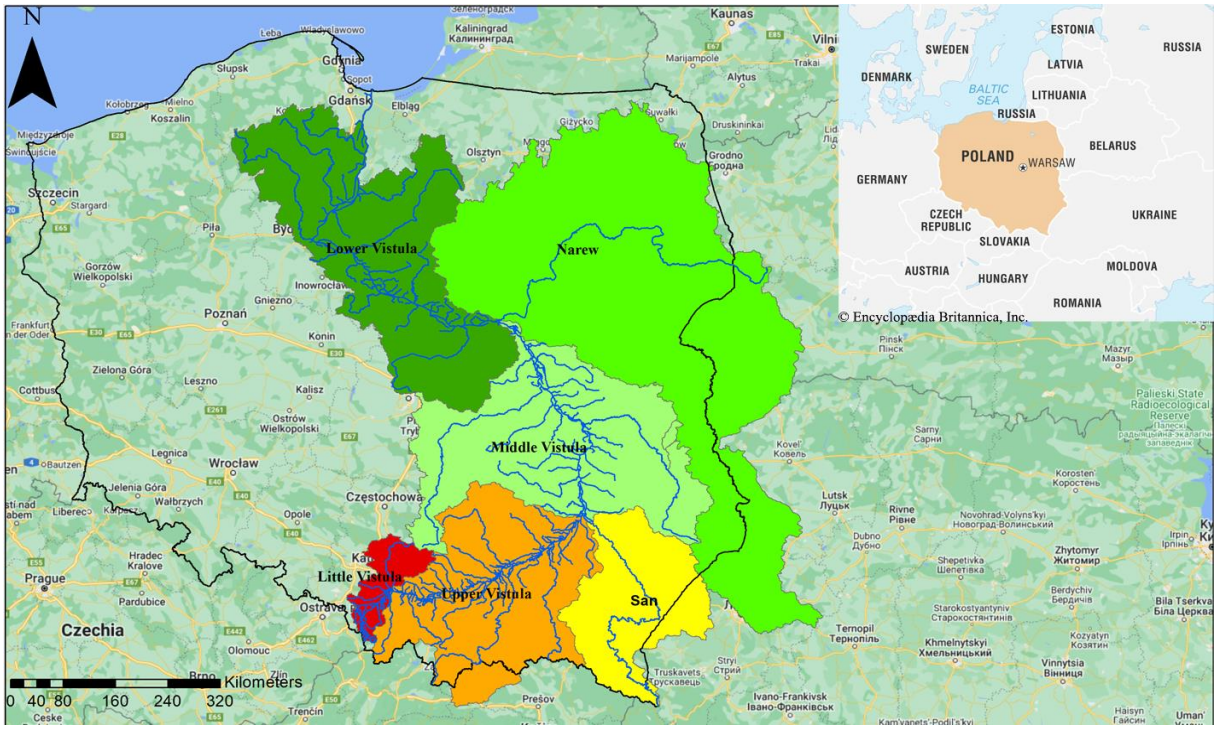

Fig. 1. Vistula basin and sub-basins.

2.2 GEE Datasets and data processing

The analysis took advantage of multiple datasets freely available via GEE, as detailed in Table 1. In particular, results extrapolated from TerraClimate are shown here.

The Palmer Drought Severity Index (PDSI), computed and released by the University of Idaho (Abatzoglou et al. 2018), uses readily available temperature and precipitation data to estimate relative dryness. In fact, it is derived by combining temperature with a physical water balance model, and therefore it can capture the basic effect of global warming on drought through changes in potential evapotranspiration.

Table 1
Used data and main information

Used data	Earth Engine Snippet	Used data range	Spatial resolution	Temporal resolution	Data reduction method
PDSI (Palmer Drought Severity Index	IDAHO_EPSCOR/ TERRACLIMATE	1958-01-01–2021-12-01	1/24°	Monthly	Monthly per basin
AET (Actual evapotranspiration)	IDAHO_EPSCOR/ TERRACLIMATE	1958-01-01–2021-12-01	1/24°	Monthly	Monthly per basin
PR (Precipitation accumulation)	IDAHO_EPSCOR/ TERRACLIMATE	1958-01-01–2021-12-01	1/24°	Monthly	Monthly per basin
RO (Runoff)	IDAHO_EPSCOR/ TERRACLIMATE	1958-01-01–2021-12-01	1/24°	Monthly	Monthly per basin
NDVI	MODIS/061/MOD13A1	2001-01-01–2021-12-01	500 m	16 days	Monthly mean per basin
EVI	MODIS/061/MOD13A1	2001-01-01–2021-12-02	500 m	16 days	Monthly mean per basin
AVERAGE, MININUM, MAXIMUM LST (Daytime Land Surface Temperature)	MODIS/061/MOD11A1	2001-01-01–2021-12-02	1000 m	Daily	Monthly mean, minimum, maximum per basin
Soil moisture (10–40 cm underground), Soil moisture (100–200 cm underground)	NASA/FLDAS/NOAH01/ C/GL/M/V001	1982-01-01–2021-12-01	1/10°	Monthly	Monthly per basin
Population density	CIESIN/GPWv411/ GPW_Population_Density	2000-01-01–2020-01-01	30″	Every 5th year	Every 5th year per basin

The PDSI is a standardized index that generally spans –10 (dry) to +10 (wet), and has been reasonably successful at quantifying long-term drought, while it has some drawbacks in quantifying sub-monthly changes, if compared with other drought indexes. As the focus of the present study is investigating long-term changes in drought-related parameters, the PDSI is assumed as a reliable proxy.

3. FIRST RESULTS

The analysis of the GEE datasets pointed out that, basin-wide, a clear increase in the drought state is visible, both in terms of severity and duration of dry conditions.

As an example, focusing on the Middle Vistula sub-basin (Fig. 2), one can notice that the PDSI observed for the last years is generally below zero, meaning drier periods, while at the beginning of the observation period (1960s and 1970s), the sub-basin was characterized by wetter conditions. Moreover, also looking at the inter-annual variations, it is possible to observe prolonged dry periods, generally not visible in the past.

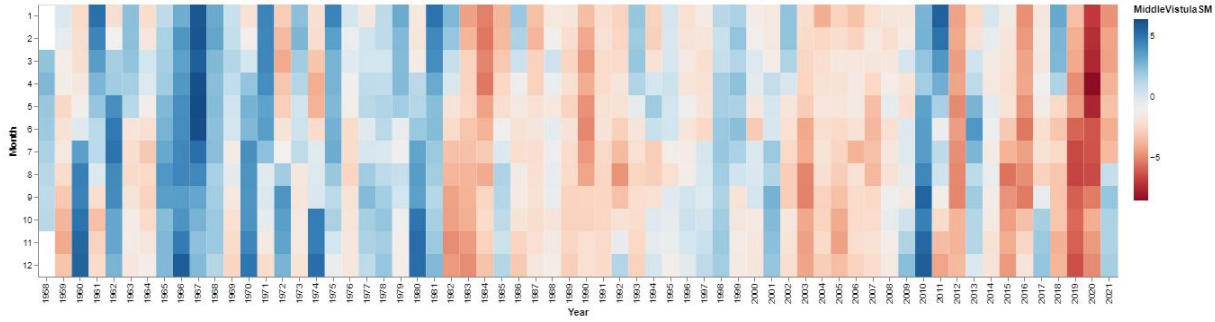

Fig. 2. Variation of the Palmer Drought Severity Index in the Middle Vistula sub-basin (derived from TerraClimate Dataset).

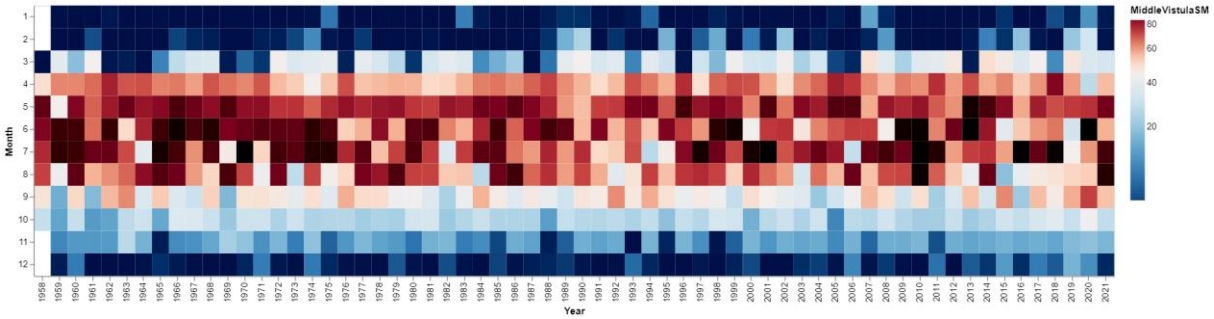

Fig. 3. Variation of actual evapotranspiration in the Middle Vistula sub-basin (derived from TerraClimate Dataset).

Looking at the actual evapotranspiration (Fig. 3) over the same sub-basin, longer periods characterized by higher evapotranspiration are observable for the last decade (see November and December). However, the dynamics observed for the PDSI are less clear in this case, suggesting that, in this case, the evapotranspiration parameter alone is not able to capture the drought phenomenon adequately.

4. CONCLUSIONS AND FUTURE PERSPECTIVES

The preliminary results presented here proved that satellite information can be used for retrieving information on drought at the basin scale, eventually providing researchers and water managers with an additional tool for locating areas where more detailed analyses are needed.

Besides analyzing past records, future investigations should be focused on understanding the drivers of the recent drought phenomena observed in the Vistula basin, via a combination of remotely acquired data with field and office information.

A c k n o w l e d g e m e n t s . This work was supported by the project HUMDROUGHT, carried out in the Institute of Geophysics of the Polish Academy of Sciences and funded by the National Science Centre (contract 2018/30/Q/ST10/00654).

Code availability: The code is available at:

https://colab.research.google.com/drive/1vCaO7z5TKRSzmQfo5WWGgQZ3D2lczDnJ

References

Abatzoglou, J.T., S.Z. Dobrowski, S.A. Parks, and K.C. Hegewisch (2018), TerraClimate, a high-resolution global dataset of monthly climate and climatic water balance from 1958–2015, *Sci. Data* **5**, 170191, DOI: 10.1038/sdata.2017.191.

Boothroyd, R.J., M. Nones, and M. Guerrero (2021), Deriving planform morphology and vegetation coverage from remote sensing to support river management applications, *Front. Environ. Sci.* **9**, 657354, DOI: 10.3389/fenvs.2021.657354.

Gorelick, N., M. Hancher, M. Dixon, S. Ilyushchenko, D. Thau, and R. Moore (2017), Google Earth Engine: Planetary-scale geospatial analysis for everyone, *Remote Sens. Environ.* **202**, 18–27, DOI: 10.1016/j.rse.2017.06.031.

Karamuz, E., and R.J. Romanowicz (2021), Temperature changes and their impact on drought conditions in winter and spring in the Vistula Basin, *Water* **13**, 14, 1973, DOI: 10.3390/w13141973.

Khan, R., and H. Gilani (2021), Global drought monitoring with big geospatial datasets using Google Earth Engine, *Environ. Sci. Pollut. Res.* **28**, 14, 17244–17264, DOI: 10.1007/s11356-020-12023-0.

Kreibich, H.; A.F. Van Loon; K. Schröter, P.J. Ward, M. Mazzoleni, N. Sairam, G.W. Abeshu, S. Agafonova, A. AghaKouchak, H. Aksoy, C. Alvarez-Garreton, B. Aznar, L. Balkhi, M.H. Barendrecht, S. Biancamaria, L. Bos-Burgering, C. Bradley, Y. Budiyono, W. Buytaert, L. Capewell, H. Carlson, Y. Cavus, A. Cousnon, G. Coxon et al. (2022). The challenge of unprecedented floods and droughts in risk management, *Nature* **608**, 80–86, DOI: 10.1038/s41586-022-04917-5.

Rakovec, O., L. Samaniego, V. Hari, Y. Markonis, V. Moravec, S. Thober, M. Hanel, and R. Kumar (2022), The 2018–2020 Multi-year drought sets a new benchmark in Europe, *Earth's Future* **10**, 3, e2021EF002394, DOI: 10.1029/2021EF002394.

Xiong, J., P.S. Thenkabail, M.K. Gumma, P. Teluguntla, J. Poehnelt, R.G. Congalton, K. Yadav, and D. Thau (2017), Automated cropland mapping of continental Africa using Google Earth Engine cloud computing, *ISPRS J. Photogramm. Remote Sens.* **126**, 225–244, DOI: 10.1016/j.isprsjprs.2017.01.019.

Received 17 November 2022
Accepted 20 December 2022

Publications of the Institute of Geophysics, Polish Academy of Sciences
Geophysical Data Bases, Processing and Instrumentation
vol. 443 (E-13), 2022, pp. 15–18
DOI: 10.25171/InstGeoph_PAS_Publs-2022-033
International Symposium on Drought and Climate Change, 24–25 November 2022

Analysis of Drought Characteristics and Associated Parameters over Indus River Basin, India

Amit DUBEY[1,✉], Deepak SWAMI[1], Vivek GUPTA[1], and Nitin JOSHI[2]

[1]Indian Institute of Technology Mandi, Mandi, Himachal Pradesh, India

[2]Indian Institute of Technology Jammu, Jammu and Kashmir, India

✉ amitd818@gmail.com

A b s t r a c t

This study is an attempt to determine the spatial-temporal pattern of meteorological droughts and exploration of the relationship between drought and elevation over Indus River basin. Gridded monthly precipitation and temperature data of 0.12°×0.12° spatial resolution for a time period of 42 years (1979–2020) is utilized. Modified Mann-Kendall test and Sen's slope method have been used to identify significant trends in the region. Drought events are identified based on Standardized Precipitation Evapotranspiration Index (SPEI) by determining of SPEI-annual and SPEI-seasonal (pre-monsoon, monsoon, post-monsoon, and winter). Results show that the trends in the drought indices have very high heterogeneity across different seasons. Overall, 13% (14%) stations show drying (wetting) trends for annual time series analysis. However, seasonally, it is found that monsoon and post- monsoon seasons have larger area in the basin with wetting trends. Moreover, pre-monsoon season have larger area with drying trends. A correlation between SPEI trends with respect to elevation is observed.

Keywords: drought, SPEI, trend analysis, elevation, Sen's slope.

1. INTRODUCTION

Drought is a natural disaster which possess a great threat to human society. The problem of water scarcity has amplified multi-folds due to coupling of effects of global warming (droughts) along with the population explosion because the available water supply is limited. Drought can

be meteorological, agricultural, and hydrological depending upon the deficiencies in precipitation, soil moisture, and stream-flow, respectively (Mishra and Singh 2010). In the recent years, the frequency of dry events has increases along with the peaks in severity as well. India is highly vulnerable to drought, occurring once in every three years from the past few decades (Mishra and Singh 2011). Drought effects various sectors especially agriculture, hence drought modelling is necessary to effectively manage the water resources. There are many indices available for quantification of drought such as Standardized Precipitation Index (SPI), Standardized Precipitation Evapotranspiration Index (SPEI), and Palmer Drought Severity Index (PDSI). Lot of studies has been carried out in India and abroad on drought characterization, drought risk including hazard and vulnerability incorporating various drought indices, but effect of topographic variable on drought dynamics is highly neglected. Feng et al. (2020) studied the effect of elevation on drought characteristics over Qinghai-Tibet Plateau and investigated that with the increase in elevation the wetting events are increasing. Similarly, drought hazard identification based on elevation and precipitation is carried out in Iran, showing decrease in drought hazard index with increasing elevation (Hosseini et al. 2020), neglecting the effect of temperature variable. Thus, current study aims to incorporate both the meteorological variable (precipitation and temperature) and develop a relation between drought and topographical variable (elevation). In this present study, Indian extent of Indus river basin has been considered as a case. Heterogeneity of the elevation spread over the basin makes it suitable for the study. Therefore, this study is an attempt to analysis the spatiotemporal variations of drought characteristics along with the exploration of relationship between dry events and topography in Indian extent of Indus River Basin.

2. STUDY AREA AND DATA

The drainage cover of Indus River basin in India has been considered in this study (Fig. 1). Indus River originates from China (Tibet) and flows through India, Afghanistan, and Pakistan covering a total basin area of 1.1 million km^2 out of which approximately 0.2 million km^2 is in India. Elevation spread of the basin shows high of 8489 m with lowest as 93 m. Meteorological gridded data (temperature and precipitation) of 0.12 degree spatial resolution for a period of 42 years (1979–2020) is acquired from National Centre for Medium Range Weather Forecasting (NCMRWF) under Ministry of Earth Sciences, India. Gridded elevation are extracted using SRTM 30 m resolution Digital Elevation Model (DEM) data from USGS earth explorer.

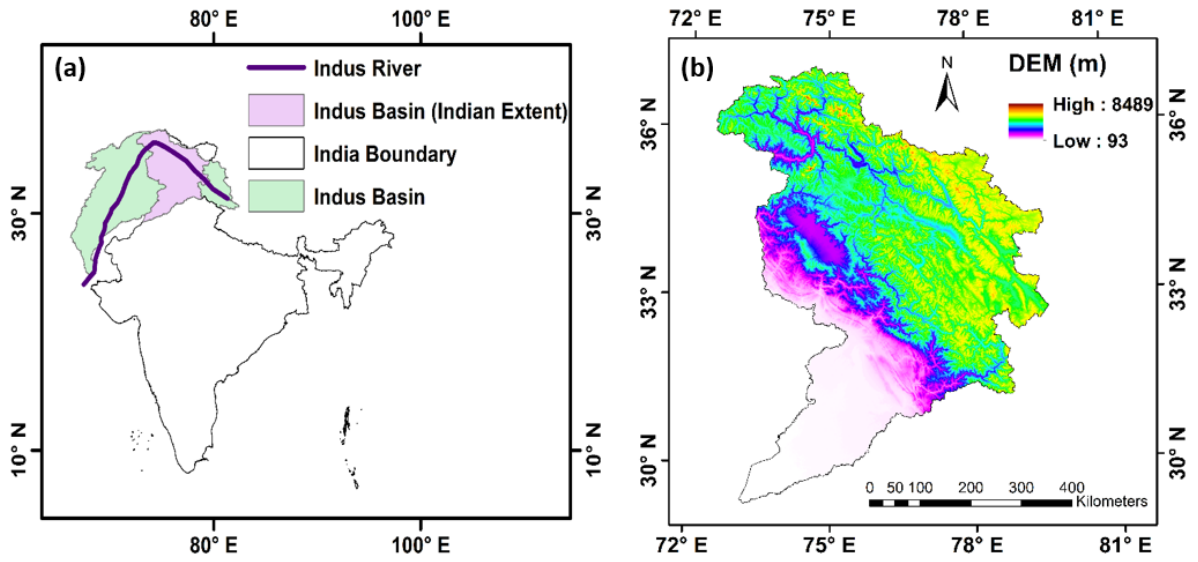

Fig. 1: (a) Study area of Indus basin, and (b) Digital Elevation Model (DEM).

3. METHODS

Standardized Precipitation Evapotranspiration Index (SPEI) is used to quantify the drought in present study. The analysis is carried out annually (June–May) and seasonally (monsoon June–September, post-monsoon October–November, winter December–February and pre-monsoon March–May). Therefore, SPEI 2, 3, 4, and 12 is computed for the entire region. SPEI is based on climatic balance equation, depending upon precipitation and Potential Evapotranspiration (PET) to identify the moisture deficiency. Hargreaves method of PET estimation has been employed, which is good option when data available is limited. Computation of SPEI and PET is done in R software using Package "SPEI". In order to detect trend in the time series, a non-parametric test called modified Mann-Kendall test at 5% significance level is used. Drawback of Mann-Kendall test includes that data has to be free from serial correlation otherwise the false rejection of hypothesis may happen, while the above limitation is rectified in modified Mann-Kendall test which is applied in R software using Package "modifiedmk". The rate at which trend increases or decreases is estimated by Sen's slope. It provides magnitude of the trend representing positive (negative) for increasing (decreasing) trend. To represent the spatial variation of Sen's slope (SPEI trends) kriging technique is applied, which is an interpolation method utilizing input as a point data and then converting into a smooth raster image.

4. RESULTS

4.1 Analysis of SPEI trends

Trend analysis on SPEI annual and seasonal time series of 1956 gridded stations have been carried out over the entire region (Fig. 2). Increasing (decreasing) trend corresponds to increase in wet (dry) events.

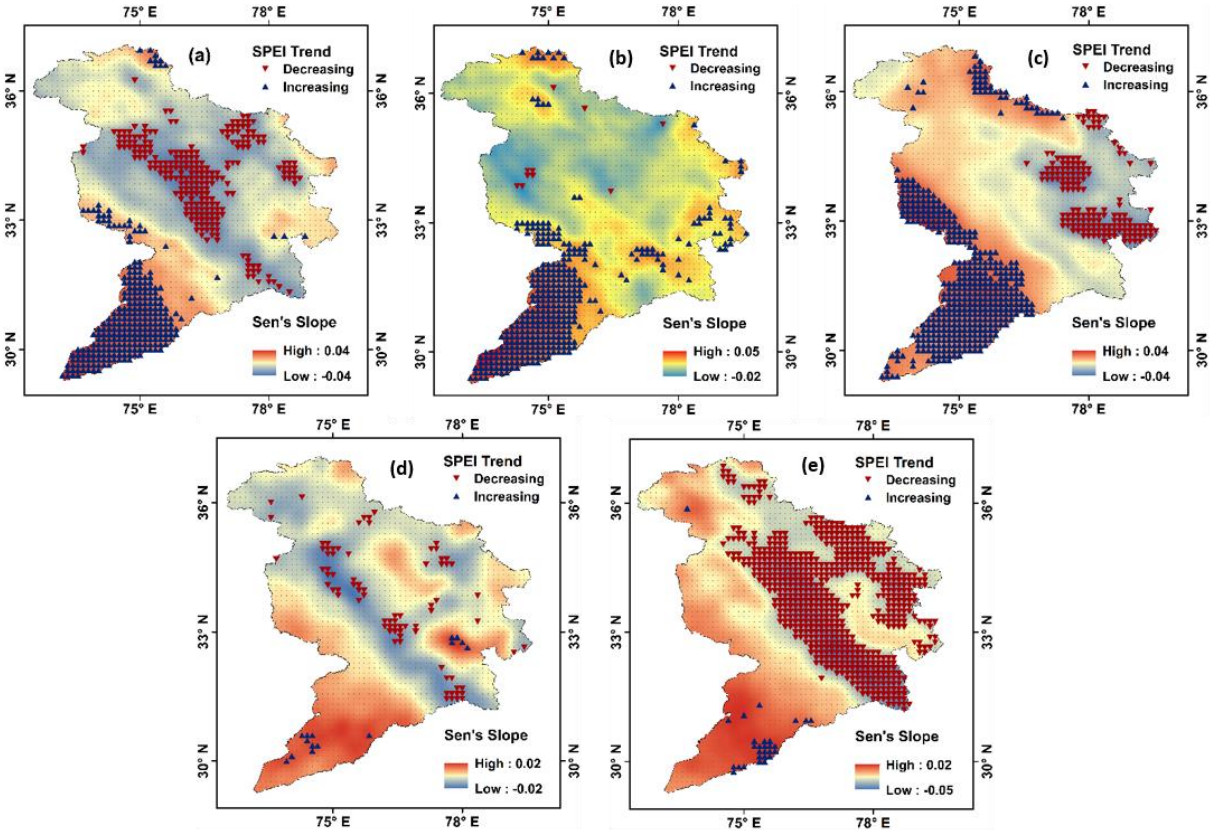

Fig. 2. Annual and seasonal distribution of SPEI trend: (a) annual, (b) monsoon, (c) post-monsoon, (d) winter, and (e) pre-monsoon.

Results show that the trends in the drought indices have very high heterogeneity across different seasons. Overall, 13% (14%) stations show drying (wetting) trends for annual time series analysis. However, seasonally, it is found that monsoon and post-monsoon seasons have larger area in the basin with wetting trends. Moreover, pre-monsoon season have larger area with drying trends, whereas, majority of the stations in winter season shows no trend.

4.2 Elevation dependence of SPEI trends

Figure 3 illustrates the relationship plot between Sen's slope of SPEI trend and elevation. Overall, it is observed that approximately up to 2000 m, wetting trends are present. Later on, with the increase in elevation the trends shift from wetting to drying corresponds to increase in dry events. Moreover, at very high altitudes above 6500 m, trends again apparently seems to decrease the drying magnitude and may attain an increasing trend.

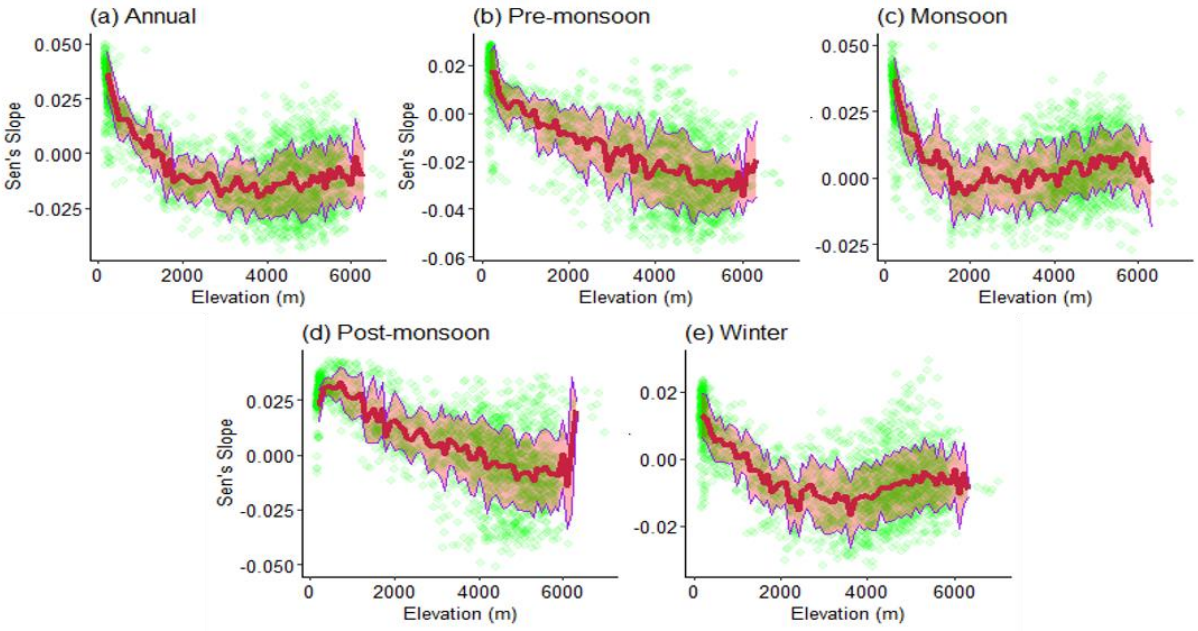

Fig. 3 Annual and seasonal relationship between SPEI trends and elevation; scatter points in green colour represents the Sen's slope of 1956 gridded stations with respect to elevation; red smooth line indicates the average of Sen's slope at every 100 m elevation interval along with the shaded area illustrating standard deviation.

References

Feng, W., H. Lu, T. Yao, and Q. Yu (2020), Drought characteristics and its elevation dependence in the Qinghai–Tibet plateau during last half-century, *Sci. Rep.* **10**, 14323, DOI: 10.1038/s41598-020-71295-1.

Hosseini, T.S.M., S.A. Hosseini, B. Ghermezcheshmeh, and A. Sharafati (2020), Drought hazard depending on elevation and precipitation in Lorestan, Iran, *Theor. Appl. Climatol.* **142**, 1369–1377, DOI: 10.1007/s00704-020-03386-y.

Mishra, A.K., and V.P. Singh (2010), A review of drought concepts, *J. Hydrol.* **391**, 1–2, 202–216, DOI: 10.1016/j.jhydrol.2010.07.012.

Mishra, A.K., and V.P. Singh (2011), Drought modeling – A review, *J. Hydrol.* **403**, 1–2, 157–175, DOI: 10.1016/j.jhydrol.2011.03.049.

Received 17 November 2022
Accepted 20 December 2022

Publications of the Institute of Geophysics, Polish Academy of Sciences
Geophysical Data Bases, Processing and Instrumentation
vol. 443 (E-13), 2022, pp. 19–19
DOI: 10.25171/InstGeoph_PAS_Publs-2022-034
International Symposium on Drought and Climate Change, 24–25 November 2022

Agricultural Drought Assessment in Nine Agricultural Regions of China through Cross-Validation of Multiple Data Products and Multiple Drought Indices

Ying PAN, Yonghua ZHU✉, and Haishen LU

Hohai University, China

✉ zhuyonghua@hhu.edu.cn

Abstract

Agricultural drought threatens global water security, food security, and human well-being. Accurate identification of agricultural drought is the premise of all work. However, it is currently challenging to achieve relatively reliable and accurate assessments using remote sensing data products. We selected soil moisture datasets from GLDAS, FLDAS, ERA5-land, and MERRA-2, precipitation from GPCC, and vegetation conditions from NDVI. Drought Severity Index (DSI), Soil Moisture Anomaly index (SMA), Standardized Precipitation Index (SPI), and Vegetation Condition Index (VCI) were calculated separately in regions with different wet and dry conditions. The objective was to find relatively reliable and accurate product and drought index by cross-validation, then apply them to agricultural drought assessment in nine agricultural regions of China. The results showed that: (1) Under different wet and dry conditions, the DSI calculated using GLDAS showed good performance in identifying agricultural drought; (2) The northern arid and semiarid region, the Northeast Plain, the Huang-Huai-Hai Plain, and the Loess Plateau frequently experienced moderate and severe agricultural droughts, especially in the region of the boundaries. Besides, the northern part of Qinghai-Tibet and the northwest region of the Yunnan-Guizhou Plateau, all with a frequency of about 20%; (3) Agricultural droughts in the agricultural regions of northern China have significantly slowed in the last 20 years, both the Yunnan-Guizhou plateau and Southern China have shown a significant increasing trend since 2002. Future agricultural droughts in the humid south need to receive more attention. This paper could help to better understand China's agricultural drought and could provide a method for agricultural drought assessment in regions without observational data.

Keywords: agricultural drought, GLDAS, DSI, nine agricultural regions, China.

Received 17 November 2022
Accepted 20 December 2022

Publications of the Institute of Geophysics, Polish Academy of Sciences
Geophysical Data Bases, Processing and Instrumentation
vol. 443 (E-13), 2022, pp. 21–21
DOI: 10.25171/InstGeoph_PAS_Publs-2022-035
International Symposium on Drought and Climate Change, 24–25 November 2022

Future Extreme Precipitation Will Be More Widespread in China under Different Global Warming Levels

Rong YU[1,✉], Panmao ZHAI[1], and Wei LI[2]

[1]Chinese Academy of Meteorological Sciences, China

[2]Nanjing University of Information Science and Technology, Nanjing, China

✉ yurong@cma.gov.cn

A b s t r a c t

CMIP6 and single model initial-condition large ensemble (SMILE) simulations are applied to find possible changes in the ratio of coverage (ROC) of extreme precipitation in China. Related results indicate that trend of ROC in the period 1961–2020 for China is underestimated by CMIP6 multi-model ensembles. Then, further analyses point out that the accuracy of model simulations to reveal a trend in observation has been improved based on the two observation constraint approaches and the SMILE-based approach. In addition, the reliability of spatial distribution has also been enhanced. Projected results indicate that ROC increases with the increment of global warming across different approaches. Among them, results based on observation constraint approaches and SMILE-based approach, which show enhanced accuracy and reliability, present larger ROC than directly using CMIP6 ensembles. Thus, it can be concluded that extreme precipitation will be more widespread in China combined with multiple evidence and methods.

Keywords: CMIP6, SMILE, projection, global warming, detection and attribution.

Received 17 November 2022
Accepted 20 December 2022

Publications of the Institute of Geophysics, Polish Academy of Sciences
Geophysical Data Bases, Processing and Instrumentation
vol. 443 (E-13), 2022, pp. 23–23
DOI: 10.25171/InstGeoph_PAS_Publs-2022-036
International Symposium on Drought and Climate Change, 24–25 November 2022

Satellite-based Soil Moisture Could Enhance the Reliability of Agro-hydrological Modeling in Large Transboundary River Basins

Mohammad Reza EINI[1,✉], Christian MASSARI[2], and Mikołaj PINIEWSKI[1]

[1]Department of Hydrology, Meteorology, and Water Management,
Institute of Environmental Engineering, Warsaw University of Life Sciences, Warsaw, Poland

[2]Research Institute for Geo-Hydrological Protection, National Research Council, Perugia, Italy

✉ mohammad_eini@sggw.edu.pl

A b s t r a c t

Satellite-based observations of soil moisture, leaf area index, precipitation, and evapotranspiration, facilitate agro-hydrological modeling thanks to the spatially distributed information. In this study, the Climate Change Initiative Soil Moisture dataset (CCI SM, a product of the European Space Agency (ESA)) adjusted based on Soil Water Index (SWI) was used as an additional (in relation to discharge) observed dataset in agro-hydrological modeling over a large-scale transboundary river basin (Odra River Basin) in the Baltic Sea region. This basin is located in Central Europe within Poland, Czech Republic, and Germany and drains water into the Baltic Sea. The Soil and Water Assessment Tool+ (SWAT+) model was selected for agro-hydrological modeling, and 26 discharge stations and soil moisture (for topsoil and entire soil profile) were calibrated for 1476 sub-basins during 1997–2019. Kling–Gupta efficiency (KGE) and SPAtial EFficiency (SPAEF) were chosen as objective functions for runoff and soil moisture calibration, respectively. Two calibration strategies were compared: one involving only discharge data (single-objective), and the second one involving discharge and satellite-based soil moisture (multi-objective). In the single-objective approach, the average KGE for discharge was above 0.60. In the multi-objective approach, the accuracy for the main discharge stations significantly increased (KGE above 0.67) compared to the single-objective approach. The results show that in this transboundary river basin, adding satellite-based soil moisture into the calibration process could improve the accuracy and consistency of agro-hydrological modeling.

Keywords: hydrology, gridded datasets, flood, drought, active and passive sensors.

Received 17 November 2022
Accepted 20 December 2022

Publications of the Institute of Geophysics, Polish Academy of Sciences
Geophysical Data Bases, Processing and Instrumentation
vol. 443 (E-13), 2022, pp. 25–25
DOI: 10.25171/InstGeoph_PAS_Publs-2022-037
International Symposium on Drought and Climate Change, 24–25 November 2022

Effects of Water Storage and Demand on Hydrological Drought Propagation in Upstream and Downstream Areas

Marco SCHILSTRA[1,✉], Wen WANG[2], Pieter VAN OEL[3], and Jingshu WANG[2]

[1]Nanjing Smart Technology Development Co. Ltd, China

[2]State Key Laboratory of Hydrology, Water Resources and Hydraulic Engineering, Hohai University, China

[3]Water Resources Management Group, Wageningen University and Research, The Netherlands

✉ schilstra49@gmail.com

A b s t r a c t

Anthropogenic factors contribute to the uneven distribution of hydrological droughts and differences in the duration and magnitude of hydrological drought in upstream and downstream areas. This study assesses how reservoir storage and water demand intensify or mitigate hydrological drought in the Shaying River basin in China. The study uses "downstreamness" as a concept to show the effect of a reservoir network on hydrological drought. For the period 1990–2018 we show that when water storage is unequally distributed between upstream and downstream areas the spatial distribution of hydrological drought also differed across upstream and downstream regions. Moreover, water demand also clearly influenced hydrological drought. Furthermore, we show a significant decreasing trend of water storage and outflow in studied reservoirs while the rates of precipitation and evaporation did not indicate a significant decreasing trend. This finding clearly shows the dominant role of human activities in intensifying hydrological drought and how this is distributed between upstream and downstream parts of a river basin. As such, this study provides useful insights that can support policymakers in formulating and evaluating drought and water policies at the river-basin scale, thus targeting solutions for both upstream and downstream areas.

Keywords: hydrological drought, reservoir operation, water demand, downstreamness, Mann-Kendall test, human activities.

Received 17 November 2022
Accepted 20 December 2022

Publications of the Institute of Geophysics, Polish Academy of Sciences
Geophysical Data Bases, Processing and Instrumentation
vol. 443 (E-13), 2022, pp. 27–27
DOI: 10.25171/InstGeoph_PAS_Publs-2022-038
International Symposium on Drought and Climate Change, 24–25 November 2022

Assessment of Drought Changes in China during 1961–2019 based on Various Indices

Pan-Mao ZHAI✉ and Chen-Peng WANG

State Key Laboratory of Severe Weather, Chinese Academy of Meteorological Sciences, Beijing, China

✉ pmzhai@cma.gov.cn

Abstract

With the aggravation of climate change, drought has become a more prominent extreme event with significant influences on both natural ecosystems and human society. The IPCC AR6 new results show that the changes in meteorological and agricultural droughts display an increasing trend in some regions. And the increasing trend shows that anthropogenic climate change plays an important role in exacerbating agricultural and ecosystem droughts. The atmospheric evaporation demand (AED) is a key variable in addressing drought change. Changes in AED are not only a direct response to climate warming, but also a driving factor for drought changes, affecting the physiological processes of vegetation.

In assessment of drought changes and their impacts, the selection of drought indices is crucial. Our study explored changes in drought condition over China and evaluated the effectiveness of four different drought indices (SPEI, SPI, MCI, and PDSI) in reflecting drought change. Four drought indices all displayed "drying trend" in North, Northeast, and Southwest China during 1961–2019. The above four indices consistently show better performance in the Middle and Lower Reaches of the Yangtze River, and in western Northwest, Northeast, and South China.

Received 17 November 2022
Accepted 20 December 2022

Publications of the Institute of Geophysics, Polish Academy of Sciences
Geophysical Data Bases, Processing and Instrumentation
vol. 443 (E-13), 2022, pp. 29–34
DOI: 10.25171/InstGeoph_PAS_Publs-2022-039
International Symposium on Drought and Climate Change, 24–25 November 2022

Quantile-quantile Correction of Satellite-based Relative Productivity in Northern Tunisia

Nesrine ABID✉ and Zoubeida BARGAOUI

University Tunis El Manar, National School of Engineers of Tunis (ENIT),
Hydraulics and Environment Laboratory (LMHE), Tunis, Tunisia

✉ nesrine_abid@ymail.com

A b s t r a c t

Satellite products such as normalized difference vegetation index (NDVI), the fraction of vegetation cover (FVC), and evapotranspiration are worth to drought assessment and alert. We consider time series of SPOT vegetation NDVI and FVC, as well as Satellite Application Facility on Land Surface Analysis (LSA SAF), reference evapotranspiration ET_0 to estimate potential evapotranspiration E_p at 3 km resolution and 10-days' time step in northern Tunisia. In addition, based on satellite LSA SAF observations of actual evapotranspiration E, we produce maps of the ratio E/E_p or relative productivity. To analyze drought conditions, we consider the time horizon from January to May relevant for cereal crops. Resulting relative productivity maps are then compared to field evidence relative to areas damaged by drought. Bias correction method is then used to correct relative productivity cumulative distribution. Results show that two thresholds are required to correct relative productivity maps to assign zero for low levels and one for high levels of relative productivity. In addition, quantile-quantile regression is worth completing relative productivity map correction.

Keywords: drought, remote sensing data, evapotranspiration, relative productivity.

1. INTRODUCTION

Drought assessment is helpful for crop yield estimation and has repercussions on the country's trade balance and food security. Satellite products are worth for assessing drought occurrence and severity. While satellite products are worth at a regional scale, they need to be analyzed at a local scale. Different methods are used for such assessment. In different parts of the world, flux tower data were used to verify the accuracy of actual evapotranspiration using as reported

from satellite observations (Cleugh et al. 2007; Paca et al. 2019). Here we propose to compare remote-sensing estimated evapotranspiration under drought conditions, with field evidence of crop damage (Abid et al. 2018). Tunisia's economy is vulnerable to drought and particularly cereal crop droughts. That's why it is challenging to use satellite products to help monitor drought and crop yield in Tunisia (Zribi et al. 2016; Chakroun 2017).

2. MATERIAL AND METHODS

2.1 Material

The study area is northern Tunisia mainly composed of three core watersheds (North Mediterranean facade watersheds called basin 3; the Medjerda basin called basin 5, and the East facade Cap-Bon and Meliane river basins called basin 4). This area covers 346 378 km². Climate conditions vary from higher humid to lower semi-arid according to Emberger index. Vegetation is composed of forest, cropland, and sparse vegetation. The study region is decomposed into 1101 units which are local administrative units called "Imada". Only 777 out of them that are non-urban areas are considered for remote-sensing estimates and field comparison. Field evidence data are obtained by analyzing the Official Journal of the Tunisian Republic where are published for each Imada the percentage of drought-damaged areas for every cereal crop campaign considering the time step from September to next May. We selected the crop campaign of 2015–2016 which is characterized by a drought that threatened more than 60% of the study area (Fig. 1). We use the variable F_a which is related to the area damaged by cereal crop drought. $F_a = 1$ returns for zero percent of the Imada's area is affected by cereal crop drought while $F_a = 0$ returns for 100 percent of the Imada's area is affected by cereal crop drought. For the period September 2015 to May 2016, we download fraction of vegetation cover FVC and normalized difference of vegetation index NDVI observations from the Copernicus SPOT-

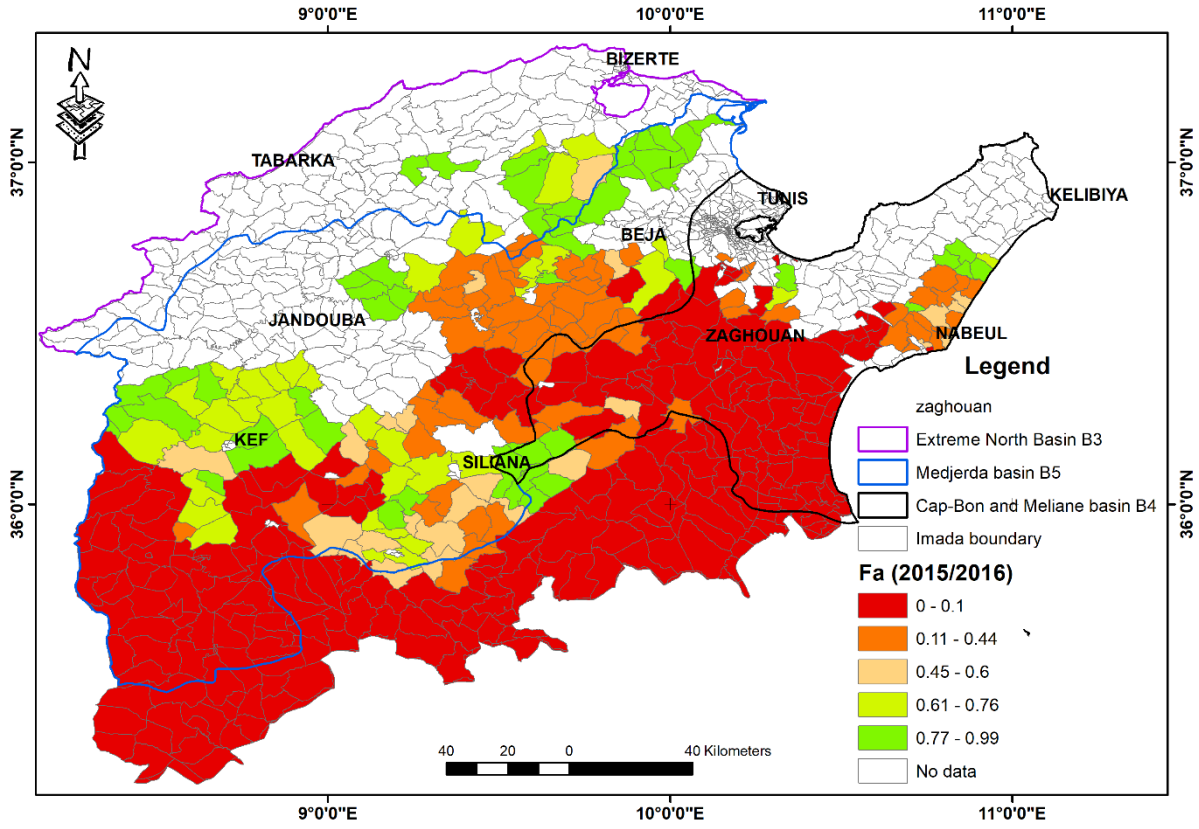

Fig. 1. Map of F_a for the 2015–2016 crop campaign.

Vegetation product with a 10-day time resolution and 1 km spatial resolution. In addition, we download actual evapotranspiration E and reference evapotranspiration ET_0 from LSA SAF products. The time resolution is daily, and the spatial resolution is 3 km. Daily E as well as daily ET_0 series are summed to obtain the totals for the period January to May 2016. Then, they are averaged over administrative entities (Imadas).

2.2 Methods

According to Eagleson (1994), for a column of atmosphere and soil of unit width, assuming the climate to be stationary, and time averaging the differential water balance equation, one obtains the climatic water balance equation:

$$P - E\,(S/\text{climate, soil, } M, k_v) - R\,(S/\text{climate, soil}) = 0 \ , \tag{1}$$

where P is the average yearly precipitation received by the surface, E – average yearly actual evapotranspiration, M – fraction of the surface covered by vegetation or canopy density, R – average yearly surface runoff, S – soil moisture state, k_v is the ratio $k_v = E/Ep$, and Ep is potential evapotranspiration also called relative productivity or crop efficiency or water stress coefficient.

As mentioned by Eagleson (1994), there are three types of functions describing productivity change versus environmental stress (S–1) distinguishing desert annual grasses and humid climate trees (Type 1) from semi-arid and subhumid trees and shrubs (Type 2) and from perennial desert plants (Type 3). Type 2's k_v varies roughly between 0.4 and 0.6 for conditions without or with small environmental stress and decreases abruptly to zero under environmental stress conditions. On Al contrary, for Type 3 the null or small stress conditions is around 0.3 while it is around 0.9 for Type 1 signifying that atmospheric demand can be met. Thus, the transpiration is much restricted for Type 3 vegetation to cope with prolonged dry periods. We assume that under semi-arid conditions of northern Tunisia Type 2 behavior holds. These permits rescaling the satellite-derived E/Ep maps using two thresholds for relative productivity. Any satellite estimated k_v less than $k_{v\min}$ is transformed to zero. Any satellite estimated k_v greater than $k_{v\max}$ is transformed to 1. Thus, $F_a = 0$ corresponds to $k_v = 0$ and $F_a = 1$ corresponds to $k_v = 1$. Then, a regression is fitted between non-transformed sample quantiles of satellite-based k_v and the fraction F_a.

We estimate the crop coefficient K_c based on the FAO-56 dual crop coefficient approach (Allen et al. 1998) which is commonly used in the literature (Er-Raki et al. 2010). K_c is calculated as a function of K_{cb} and K_e (Rocha et al. 2010; Abid et al. 2018):

$$K_c = K_{cb} + K_e \ , \tag{2}$$

where K_{cb} is crop transpiration coefficient, K_e – soil evaporation fraction, K_{cb} – a function of NDVI, and K_e is a function of FVC (Rocha et al. 2010; Abid et al. 2018).

The potential evapotranspiration is evaluated using Eq. (3):

$$E_p = K_c * ET_0 \ . \tag{3}$$

Pixels E_p are first summed to obtain the January to May 2016 totals. Then, they are averaged over administrative entities (Imadas) and the ratio E/E_p is estimated for every entity. Its relevance is assessed in comparison to the fraction F_a informing about the percent of the area damaged by drought for cereal crops ($F_a = 0$ corresponds to 100% of the Imada affected by cereal crops). A statistical analysis of the sample cumulative distribution of F_a and satellite-based k_v is undertaken. Bias correction is achieved using the two above mentioned thresholds for satellite-based k_v as well as quantile-quantile regression (Piani et al. 2010).

3. RESULTS

Figure 2 shows the scatterplot of actual evapotranspiration averaged by Imada in comparison to potential evapotranspiration. Per Imada, in the period January–May 2016 total actual evapotranspiration vary between 20 and 200 mm while potential evapotranspiration is between 175 and 300 mm. Figure 3 shows the map of estimated k_v for the period from January to May 2016.

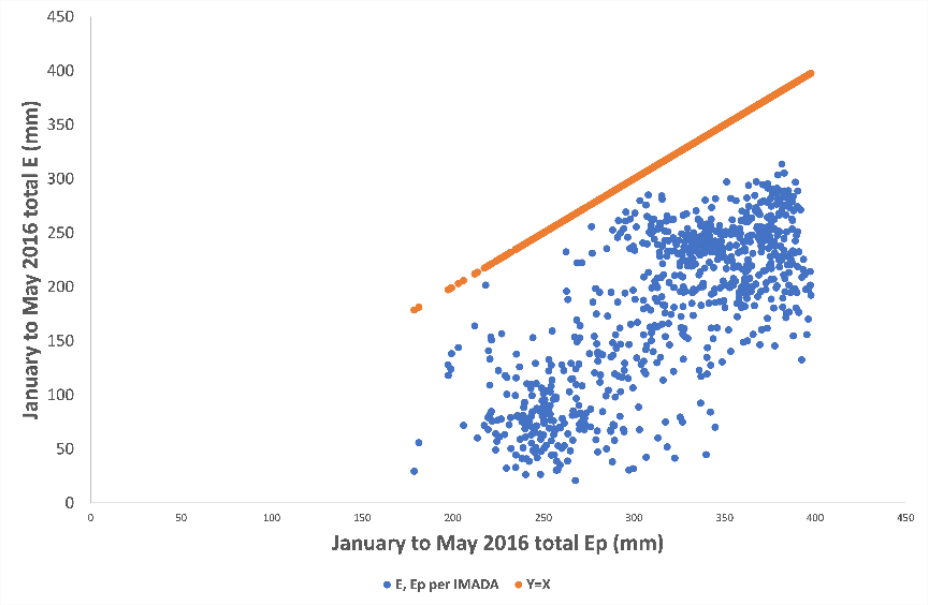

Fig. 2. Scatter plot for actual and potential evapotranspiration (January to May 2016) per Imada.

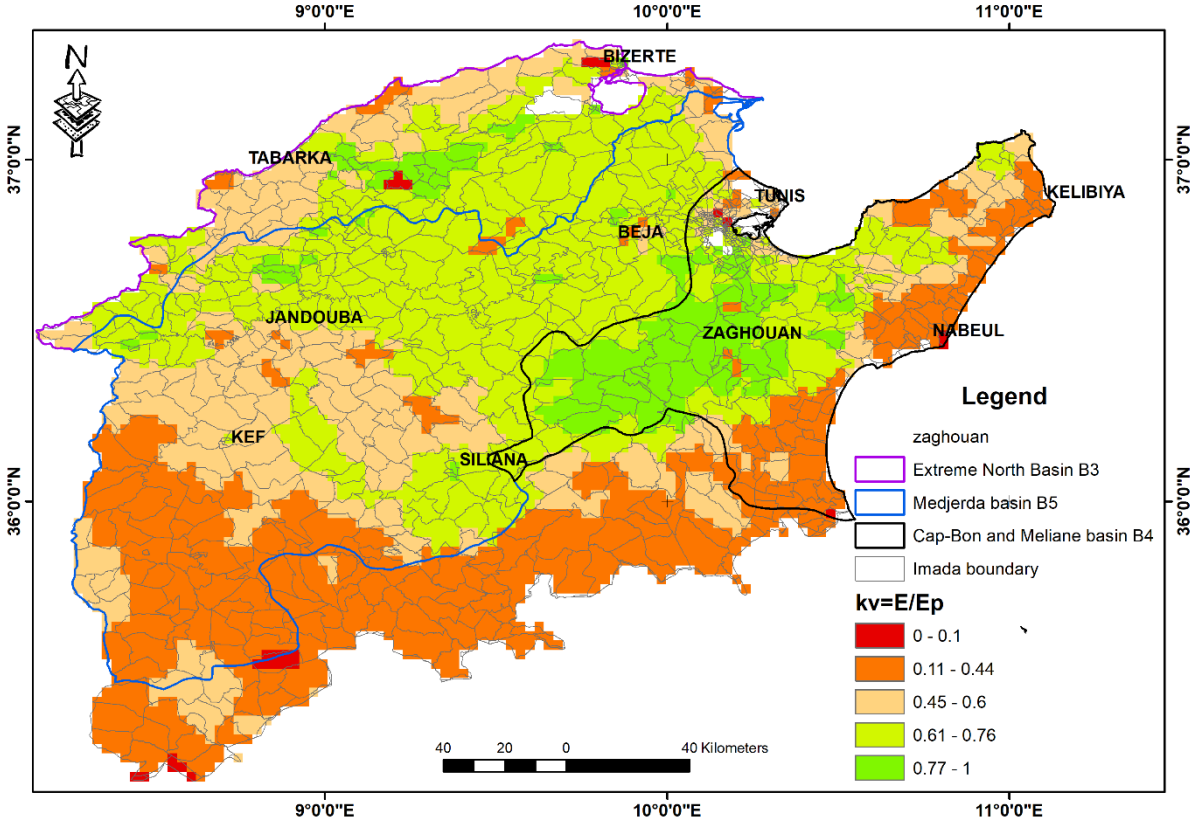

Fig. 3. Spatial distributions of k_v.

The sample distributions of ranked k_v and F_a are shown in Fig. 4. There is clearly a need for bias correction. Based on Fig. 4, the following thresholds are assumed: $k_{v\min} = 0.45$ and $k_{v\max} = 0.62$. Thus, for every Imada with raw $k_v < 0.45$ the transformed $k_v = 0$. Similarly, for every Imada with raw $k_v > 0.62$ the transformed $k_v = 1$. Otherwise, raw k_v are ranked as well as corresponding F_a. Quantile-quantile regression is then achieved (Fig. 5). As seen in Fig. 5, the regression is with very good accuracy helping drought impact investigation in northern Tunisia.

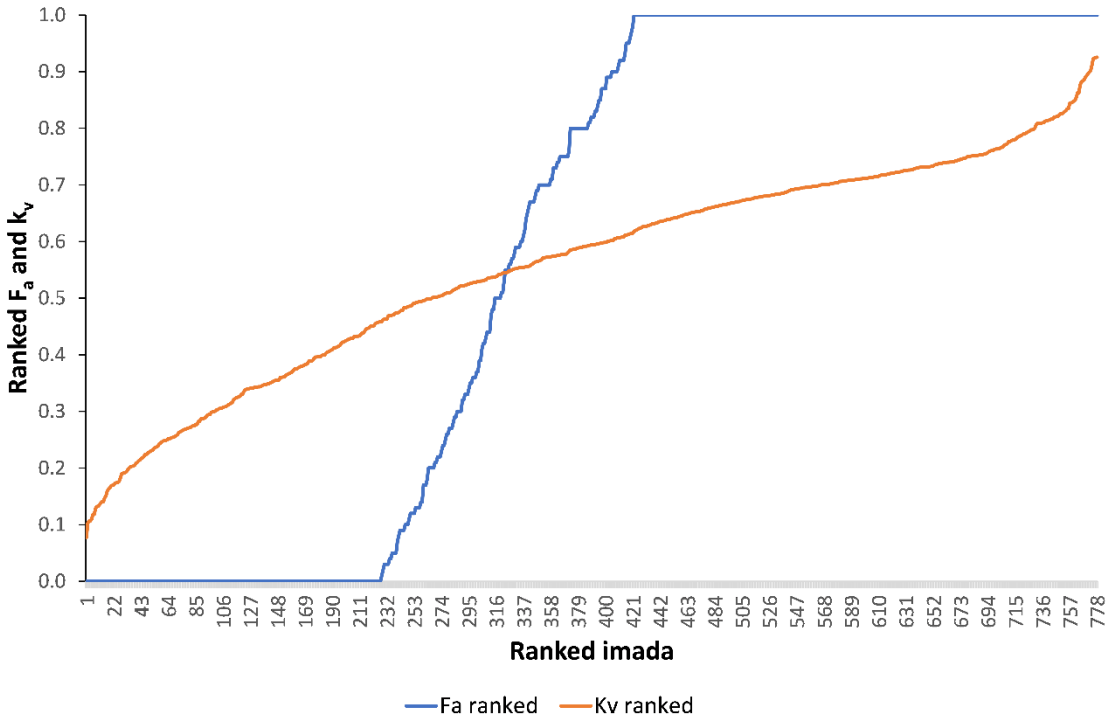

Fig. 4. Cumulative distributions of F_a and raw k_v.

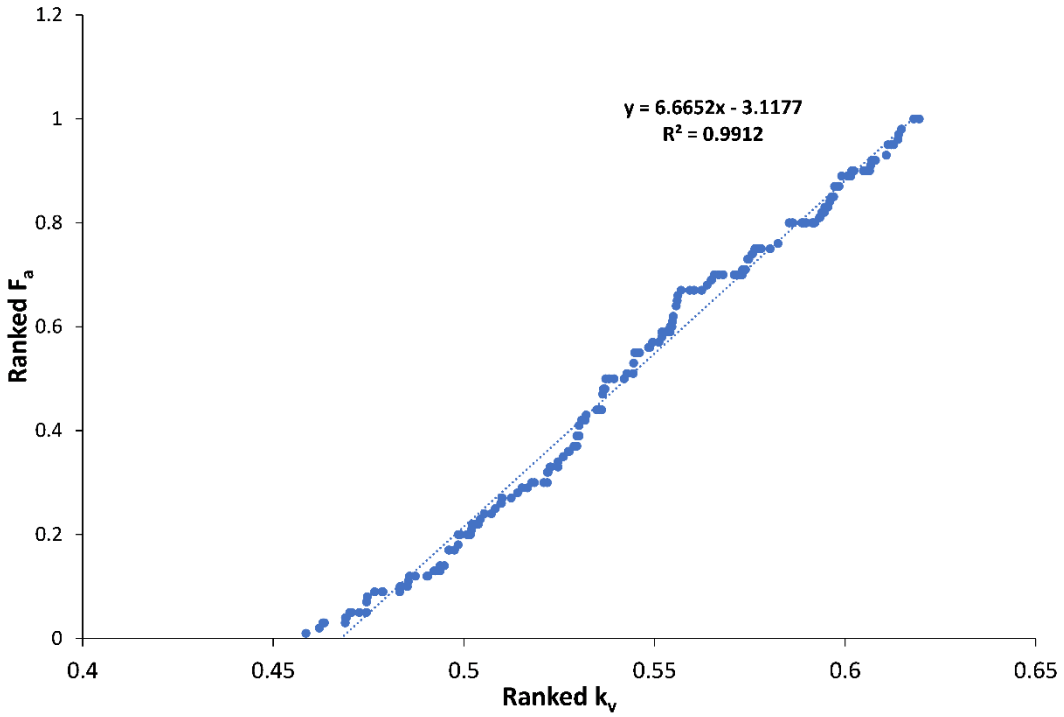

Fig. 5. Quantile-quantile regression between F_a and non-transformed k_v.

4. CONCLUSION

For Northern Tunisia and the drought occurred in the crop campaign 2015–2016, the field assessment achieved by the Tunisian authorities to estimate the percentage of the affected area by drought for every administrative unity at the local scale (Imada), is compared to the crop productivity calculated using remote sensing data and products from SPOT and LSA SAF. Bias correction using quantile-quantile regression resulted in a very good accuracy between the two derived maps. Therefore, the perspective is to evaluate the relevance of other periods for drought mitigation as well as to analyze other drought events and non-drought periods.

Acknowledgments. This work is under the national project PAQ-Collabora entitled "Monitoring/development of drought indices for decision support concerning the management of cereal productivity in Tunisia". We thank the Ministry of High Education for this funding.

References

Abid, N., Z. Bargaoui, and C.M. Mannaerts (2018), Remote sensing estimation of the water stress coefficient and comparison with drought evidence, *Int. J. Remote Sens*. **39**, 14, 4616–4639, DOI: 10.1080/01431161.2018.1430917.

Allen, R.G., L.S. Pereira, D. Raes, and M. Smith (1998), Crop evapotranspiration – Guidelines for computing crop water requirements, FAO Irrigation and Drainage, Paper no. 56, FAO Rome, available at: http://www.fao.org/docrep/X0490E/X0490E00.html.

Chakroun, H. (2017), Quality assessment of MODIS time series images and the effect on drought monitoring, *Open J. Appl. Sci*. **7**, 7, 365–383, DOI: 10.4236/ojapps.2017.77029.

Cleugh, H.A., R. Leuning, Q. Mu, and S.W. Running (2007), Regional evaporation estimates from flux tower and MODIS satellite data, *Remote Sens. Environ.* **106**, 3, 285–304, DOI: 10.1016/j.rse.2006.07.007.

Eagleson, P.S. (1994), The evolution of modern hydrology (from watershed to continent in 30 years), *Adv. Water Resour*. **17**, 1–2, 3–18, DOI: 10.1016/0309-1708(94)90019-1.

Er-Raki, S., A. Chehbouni, G. Boulet, and D.G. Williams (2010), Using the dual approach of FAO-56 for partitioning ET into soil and plant components for olive orchards in a semi-arid region, *Agr. Water Manage*. **97**, 11, 1769–1778, DOI: 10.1016/j.agwat.2010.06.009.

Paca, V.H., G.E. Espinoza-Dávalos, T.M. Hessels, D.M. Moreira, G.F. Comair, and W.G.M. Bastiaanssen (2019), The spatial variability of actual evapotranspiration across the Amazon River Basin based on remote sensing products validated with flux towers, *Ecol. Process*. **8**, 6, DOI: 10.1186/s13717-019-0158-8.

Piani, C., J.O. Haerter, and E. Coppola (2010), Statistical bias correction for daily precipitation in regional climate models over Europe, *Theor. Appl. Climatol*. **99**, 187–192, DOI: 10.1007/s00704-009-0134-9.

Rocha, J., A. Perdigão, R. Melo, and C. Henriques (2010), Managing water in agriculture through remote sensing applications. **In:** R. Reuter (ed.), *Proc. 30th EARSeL Symposium on Remote Sensing for Science, Education, and Natural and Cultural Heritage, Paris, France*, Vol. 31, 223–230, available from: https://www.researchgate.net/profile/Jorge_Rocha7/publication/228413258_Managing_Water_in_Agriculture_through_Remote_Sensing_Applications/links/00b7d533e978b95954000000.pdf.

Zribi, M., G. Dridi, R. Amri, and Z. Lili-Chabaane (2016), Analysis of the effects of drought on vegetation cover in a Mediterranean Region through the use of SPOT-VGT and TERRA-MODIS long time series, *Remote Sens*. **8**, 12, 992, DOI: 10.3390/rs8120992.

Received 17 November 2022
Accepted 20 December 2022

Publications of the Institute of Geophysics, Polish Academy of Sciences
Geophysical Data Bases, Processing and Instrumentation
vol. 443 (E-13), 2022, pp. 35–39
DOI: 10.25171/InstGeoph_PAS_Publs-2022-040
International Symposium on Drought and Climate Change, 24–25 November 2022

Conceptual Approach for a Holistic Low-Flow Risk Analysis

Udo SATZINGER✉ and Daniel BACHMANN

University of Applied Sciences Magdeburg-Stendal,
Department of Water, Environment, Construction and Safety, Magdeburg, Germany

✉ udo.satzinger@h2.de

A b s t r a c t

The recent drought events highlighted the impacts caused by hydrological drought and low-flow events to society and ecosystems. In Germany, some rivers even dried out during the drought events of 2018, 2019, and 2022 causing massively damages to the ecosystem. Also, the impact on the economy due to restrictions on water use is immense. In this work we present a conceptual approach for a holistic low-flow risk analysis as base for an effective risk management including risk acceptance, transparent evaluation of mitigation measures and communication. The low-flow risk combines probabilities and consequences of low-flow events on a (sub-)catchment scale. However, the risk analysis is based on synthetic long-term time series (continuous risk modelling), as these appear to be more suitable for low-flows than scenario-based simulations, which are well known from flood risk analysis. The holistic approach requires a representation of all relevant processes, starting from weather generation, the hydrological and hydrodynamic response, and the consequences to society and ecosystems.

Keywords: low-flow risk analysis, hydrological drought, drought management, risk analysis.

1. INTRODUCTION

The drought events of 2018 and 2019 have shown the massive impact of hydrological drought and the resulting low-flows on water users all over Europe. The drought situation in summer 2022 again provided low water levels with several new negative record values and massive restrictions on water use. In France, the water temperature in some rivers exceeded the specified threshold values, hence nuclear power plants were only allowed to continue using cooling water with special permits (Markert 2022; tagesschau 2022). In many parts of Germany private water withdrawal from surface water was prohibited (MDR 2022a, b). Shipping on the Rhine was

disturbed for several weeks in July and August 2022, leading to disrupted supply chains and higher freight costs (tagesschau 2022). The river Schwarze Elster in southern Brandenburg and the river Dreisam in Baden-Württemberg partly dried out (DPA 2022; Bergmann 2022). The ecological losses in these dry sections are massive and full recovering will take years. In other rivers the high water temperatures lead to a lack of oxygen and cause ecological impact (Höger et al. 2022).

The impact of recent events demonstrates the urgent need for effective low-flow risk management, particularly by an expected future increase of these events due to climate change. All tasks within low-flow risk management are based on a well-founded risk analysis, combining probabilities and impact of low-flow events in a quantitative way. A holistic risk analysis approach is required to represent all relevant processes leading to consequences. The results as risk values support transparently the risk acceptance process and communication task as well as the conceptual design and evaluation of mitigation measures. This includes administrative measures like prioritizing and coordinating of individual water users during low-flow events, measures of storage as adapted reservoir management or constructive measures like low-water channels in a river. Finally, a software tool is required which transfers the application of a low-flow risk analysis to the end-users.

2. METHOD: HOLLISTIC LOW-FLOW RISK APPROACH

The low-flow risk analysis approach focusses on so-called blue-water droughts and their consequences, following the definition in Speed et al. (2016) as "unusual and significant deficiency in the water stored in freshwater lakes, rivers, aquifers, and wetlands". Rivers and their surrounding areas are target areas. Low water levels and high water temperatures resulting in ecological and economic consequences are analysed.

In the field of flood risk applications, scenario-based calculations are often performed. For example, the relevant parameter for the design of flood protection structures as levees is based on HQ100, a discharge that statistically occurs once in 100 years. Flood hazard maps are calculated for three different scenarios. Due to a relative short duration of flood events between a few days to a few weeks and in general negligible hydrological interaction between temporal distant flood events, a clear distinction of such events is comparatively simple.

However, for low-flow risk modelling, the definition of scenarios is considerably more complex due to their long-term development and occurrence. While in a river flood the hydrological situation of the previous year has just a negligible impact on the characteristics of the flood event, low-flow, in contrast, is a gradual process that develops over weeks, months and years. Thus, hydrological conditions from previous years can be essential for the development of a low-flow event.

Therefore, a long-term simulation approach is proposed for the low-flow risk analysis. The fundamental model concept is adapted from a long-term approach applied in flood risk analysis research, further described in Sairam et al. (2021). The basic idea consists not on the selection of independent scenarios, it is based on the generation of synthetic long-term time series (continuous risk modelling) from several hundred or thousand years, including weather generation, hydrology (Hydrological module), hydrodynamic (Hydrodynamic module), and analysis of consequences (Consequences module, cp. Fig. 1). The risk, finally, is calculated by the sum over the consequences divided by the simulated years (Risk module). This continuous approach makes it possible to fully represent the temporal connected low-flow events with their characteristics and consequences within the risk calculation. Considering low-flow events this approach is clearly advantageous compared to the scenario-based approach.

In the following a short description of the individual modular components of the holistic approach and their connections are given. In a first step a statistical weather generator is applied

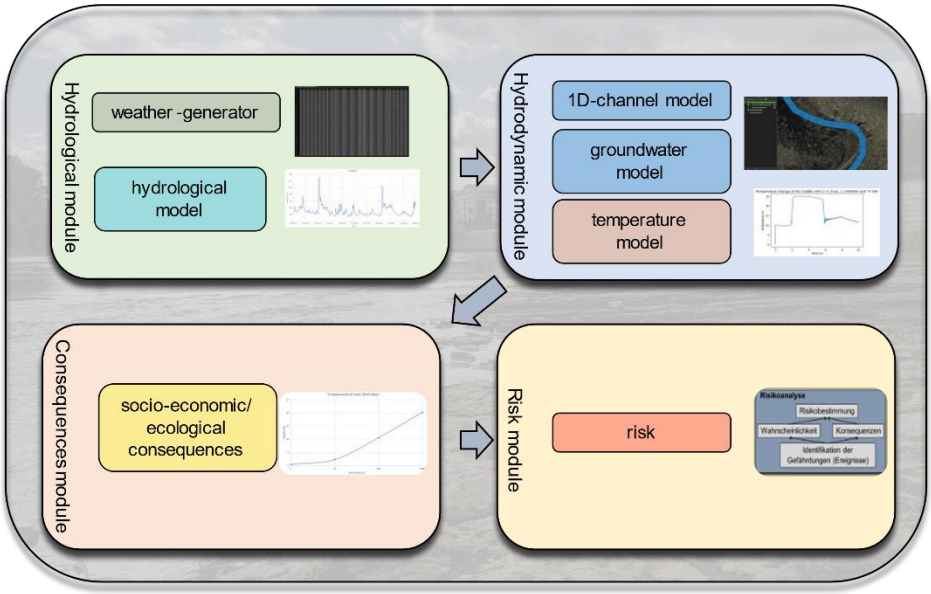

Fig. 1. Conceptual model approach for a holistic low-flow risk analysis.

(cp. Fig. 1) to produce synthetic long time series of relevant weather parameters (like precipitation, temperature, etc.) based on the statistical description of the current climate. This generated weather data serves as input data for the hydrological model of a river catchment. The hydrological model calculates the required results, such as runoff and infiltration.

Area-specific influencing factors such as land use, topography, and soil type of the area under investigation are considered.

The hydrodynamic module uses the results of the hydrological model as input. It consists of three submodules. The core of the module is the one-dimensional river model, which models, e.g., water levels and flow velocities in the river on basis of the diffusive wave approach (a simplification of the St. Venant-equations). In addition to hydrological data, input data such as cross section geometry and friction coefficients are considered. The hydrodynamic module also includes a model of the near-surface groundwater body. It is used to model the groundwater levels in the vicinity of the river. The groundwater model is coupled bidirectionally to the river model. In this way, the interaction of the groundwater and the river through ex- and infiltration can be modelled realistically. Last step in the hydrodynamic analysis of the river is the calculation of water temperature as a possible indicator of water quality. The coupling to the hydrodynamic river model is unidirectional. After its calculation is completed, the results of the river model, especially the flow velocity, are transferred to the temperature model. As further input global radiation and characteristics of anthropogenic inlets are integrated.

Based on the results of the hydrodynamic module, the consequences of low-flow for the different water users and the river ecosystem are quantified. The determination of the consequences is very complex, because the effects are manifold (e.g., Folkens et al. (2022)). The basic principle of the assessment of socio-economic consequences is based on threshold values above which a consequence occurs. As an example, the shipping industry can only operate with reduced freight at defined water levels. The situation is similar for power plants, which are only allowed to draw water for cooling purposes to a limited extent if the water temperature exceeds a certain threshold. A pure monetary evaluation is possible. The ecological consequences are evaluated using fixed empirical values. For example, many fish only can tolerate a water temperature of over 28°C for a short period of time. If for the ecological consequences a monetary assessment is adequate needs to be further developed. As a result, the accumulated sum of damages of the analysed long-term time series – including low flow events - are determined.

3. RESEARCH PROJECT DRYRIVERS

This work is part of the DRYRIVERS research project, which aims to develop a tool for effective low-flow risk management. The tool will be tested in the pilot areas of the river Selke, Rur, and a part of the Elbe river. In addition to the risk analysis, mitigation measures and mitigation strategies will be developed. An overview of the project is presented in Bachmann et al. (2022). The project, which is being conducted by interdisciplinary partners from the University of applied sciences Magdeburg-Stendal, RWTH Aachen University, the umweltbüro Essen, and LimnoPlan, started in February 2022 and will run until the beginning of 2025.

4. CONCLUSION

Recent drought events highlighted the massive economic and ecological impacts of hydrological drought. Approaches and tools are required to effectively support the management of these extreme events. Thus, we present a holistic risk analysis approach for a basic support of a low-flow risk management. It considers all relevant processes from the weather-generation to consequences to ecosystems and society, mirroring the holistic set-up. The modelling is performed using long-term series, which are more suitable for analysing low-flow events than an event-based approach. In the flowing steps of DRYRIVERS this developed conceptual approach will be implemented in a tool and tested at three river catchments in Germany.

Acknowledgments. This research is funded within the research framework of WaX (Wasser-Extremereignisse) by the Federal Ministry of Education and Research of Germany.

References

Bachmann, D., H. Schüttrumpf, S. Staas, M. Halle, and T. Franke (2022), DRYRIVERS – Ziele, Anforderungen, Strategien und Werkzeuge für ein zukunftsfähiges Niedrigwasserrisikomanagement (NWRM), available from: https://www.researchgate.net/publication/360320695_DRYRIVERS_-Ziele_Anforderungen_Strategien_und_Werkzeuge_fur_ein_zukunftsfahiges_Niedrigwasserrisikomanagement_NWRM (accessed: 19.09.2022) (in German).

Bergmann, J. (2022), Blanker Stein, tote Insekten – Dreisam früher als sonst auf dem Trockenen, SWR Aktuell, available from: https://www.swr.de/swraktuell/baden-wuerttemberg/suedbaden/trockenheit-fluss-dreisam-100.html (accessed: 12.07.2022) (in German).

DPA (2022), Klima: Flüssen fehlt Wasser, Angespannte Lage an Schwarzer Elster, Deutschen Presse-Agentur, Die Zeit, available from: https://www.zeit.de/news/2022-07/19/fluessen-fehlt-wasser-angespannte-lage-an-schwarzer-elster?utm_referrer=https%3A%2F%2Fwww.google.com%2F (accessed: 19.07.2022) (in German).

Folkens, L., T. Franke, L. Heermann, S. Staas, L. Sollinger, M. Halle, D. Bachmann, P. Schneider, and V. Wiedemer (2022), Poster DryRivers: Ökologische & ökonomische Niedrigwasserrisiken, available from: https://www.researchgate.net/publication/360342664_Poster_DryRivers_Okologische_okonomische_Niedrigwasserrisiken (accessed: 19.09.2022) (in German).

Höger, S., Br24 Redaktion, and M. von Lieben (2022), Warme Flüsse werden zur Belastung für Fische, BR24, available from: https://www.br.de/nachrichten/bayern/warme-fluesse-werden-zur-belastung-fuer-fische,TCmE1m4 (accessed: 28.07.2022) (in German).

Markert, S. (2022), Frankreich: Zwischen Kernkraft und Klimawandel, tagesschau.de, available from: https://www.tagesschau.de/ausland/europa/frankreich-atomkraft-natur-101.html (accessed: 10.08.2022) (in German).

MDR (2022a), Wasserentnahme verboten: Das gilt in Sachsen-Anhalts Landkreisen, Mitteldeutscher Rundfunk (MDR), available from: https://www.mdr.de/nachrichten/sachsen-anhalt/wasser-entnahme-verboten-fluesse-garten-100.html (accessed: 10.07.2022) (in German).

MDR (2022b), Wasserentnahme-Verbote: Was gilt wo? Mitteldeutscher Rundfunk (MDR), available from: https://www.mdr.de/ratgeber/recht/wasserentnahme-verboten-uebersicht-regeln-100.html (accessed: 14.08.2022) (in German).

Sairam, N., F. Brill, T. Sieg, M. Farrag, P. Kellermann, V.D. Nguyen, S. Lüdtke, B. Merz, K. Schröter, S. Vorogushyn, and H. Kreibich (2021), Process-Based Flood Risk Assessment for Germany, *Earth's Future* **9**, 10, e2021EF002259, DOI: 10.1029/2021EF002259.

Speed, R., D. Tickner, G. Lei, P. Sayers, Y. Wei, Y. Li, C. Moncrieff, G. Pegram, J. Li, X. Xu, A. Li, and B. Qiu (2016), *Drought Risk Management. A Strategic Approach*, UNESCO Publishing, Paris, 215 pp.

tagesschau (2022), Pegelstände am Rhein: Niedrigwasser belastet deutsche Wirtschaft, tagesschau.de, available from: https://www.tagesschau.de/wirtschaft/unternehmen/niedrigwasser-rhein-wirtschaftliche-auswirkungen-101.html (accessed: 05.08.2022) (in German).

Received 17 November 2022
Accepted 20 December 2022

Publications of the Institute of Geophysics, Polish Academy of Sciences
Geophysical Data Bases, Processing and Instrumentation
vol. 443 (E-13), 2022, pp. 41–46
DOI: 10.25171/InstGeoph_PAS_Publs-2022-041
International Symposium on Drought and Climate Change, 24–25 November 2022

The Dynamics of Low Flows Characteristics and Exposure to Hydrological Drought along the River Vistula and in its Basin

Ewa BOGDANOWICZ✉, Emilia KARAMUZ, Iwona MARKIEWICZ,
and Krzysztof KOCHANEK

Department of Hydrology and Hydrodynamics, Institute of Geophysics,
Polish Academy of Sciences, Warsaw, Poland

✉ ewabgd@igf.edu.pl

A b s t r a c t

The process of propagation of low flows is studied in the River Vistula in Poland. A history of low flow events in the basin is derived on the basis of statistical analysis of flow measured at 15 gauging stations located along the river and in 12 stations on its main tributaries in the 1951–2018 period. The main characteristics of low flows: minimum flow, duration and deficit of flow are calculated and analysed (at-side trend analysis, variability with the course of the river). On this base the most severe low flows are listed at each gauging stations and on the Little, Upper, Middle, and Lower Vistula reaches. The method of QdF (flow-duration-probability) was used to estimate the flow non-exceeded in *d*-days with the probability 50% and the index of low flow dynamics *D*. The results are compared in time and along the river. The exposure to drought are examined in terms of temporal and spatial aspects.

Keywords: low flows, the Vistula basin, statistical analysis, temporal and space exposure to drought.

1. INTRODUCTION

In Poland, there are two types of low flows of different origin. The summer low flows, preceded by atmospheric and soil drought, begin with a depletion of the catchment retention resources. Summer low flows are generally long-lasting, large-scale, and dominant in the lowland part of the country. They often extend into the autumn period and are then called summer–autumn low flows posing a long-term important threat to the water supply for the population, industry, and agriculture. The end of the summer low flow is most often associated with the occurrence of precipitation and a reduction in evapotranspiration.

Winter low flows are characteristic mainly in mountain rivers, although they can also occur in lowland rivers. Their occurrence is associated with longer periods of negative air temperature. In those conditions the surface runoff is stopped and inflows of groundwater to the riverbeds are strongly reduced (Dębski 1967; Fal 2007; Hydrologia 2017).

This research was carried out to resolve several important issues regarding the low flows on the Vistula:

- Is the combined impact of climatic change and human activities revealed in the long-term series of low flow characteristics in the Vistula and its basin and what form does that impact take?
- Which characteristics of the low flow regime are most affected and where?
- What are the time frames of low flows on the Vistula and the areas prone to drought?

2. DATA AND METHODS

2.1 Study area

This study covers the River Vistula from its sources to the hydrological station in Tczew (closing station) presented in Fig. 1.

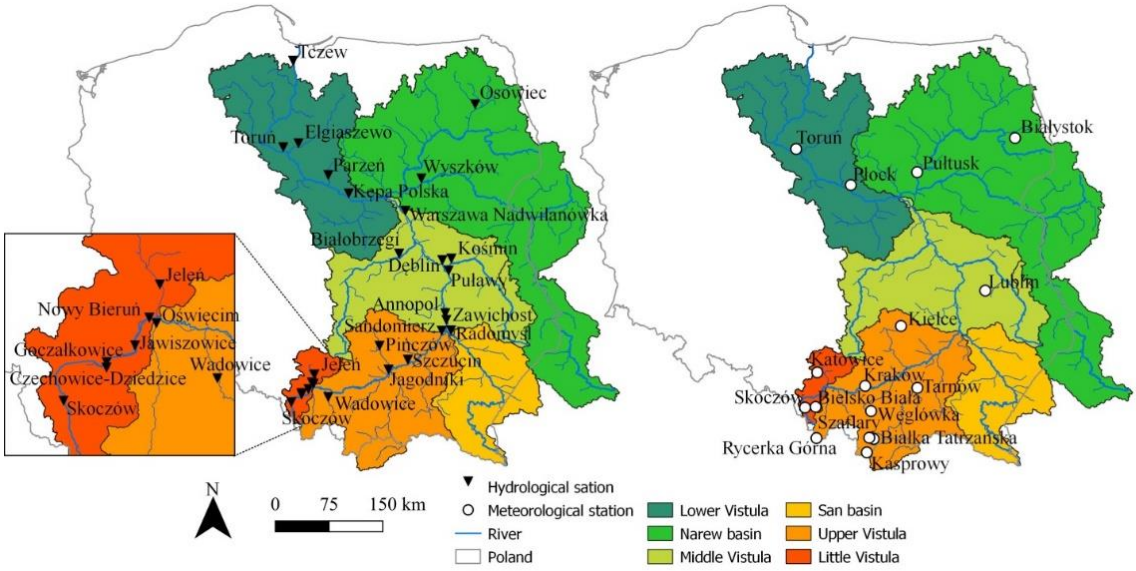

Fig. 1. The River Vistula basin with location of hydrological stations used in the study (Bogdanowicz et al. 2021).

2.2 Methodology

The lowest annual flow, still often used in Polish hydrological practice, was adopted as the threshold of the low flow event. Several days of higher flow periods (2–5 days) have been included (Fal 2007). The flow minima, deficits and durations were calculated and their trends are estimated. The flow-duration-probability (QdF) model were used to estimate design characteristics. The method for time and space exposure to droughts to point the most potentially affected areas.

3. PRELIMINARY RESULTS AND CONCLUSIONS

The results concern three problems formulated in the introductory section. The combined impact of climatic change and human activities in seasonal minima is depicted in Fig. 2. in the form of linear trends in the mean value and standard deviation estimated by means of the method proposed by Strupczewski and Kaczmarek (2001).

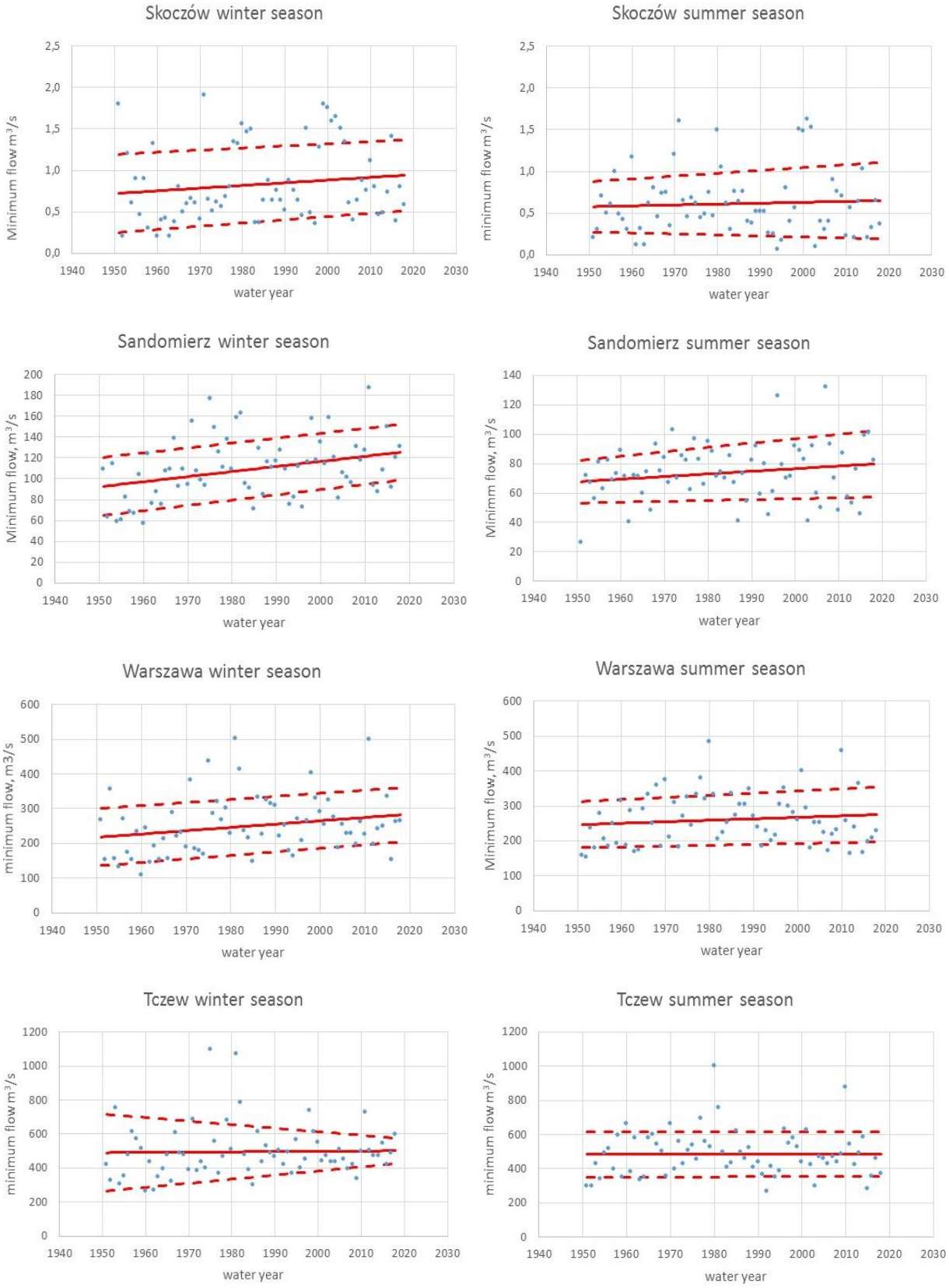

Fig. 2. Trends in mean seasonal minimum flow (red line) and standard deviation (dashed line).

Analyzes of trends in many outflow characteristics have shown, inter alia, that the minimum winter flows increased in the period 1951–2018. In general, the summer minima do not show a downward trends (Bogdanowicz et al. 2021).

The exemplary result of QdF (i.e., low flow dynamics parameter *D*, the flow non-exceeded in 10 days with probability 50% – $Q_{10,50\%}$ and the mean annual lowest flow (mean LQ), modelling are presented in Fig. 3.

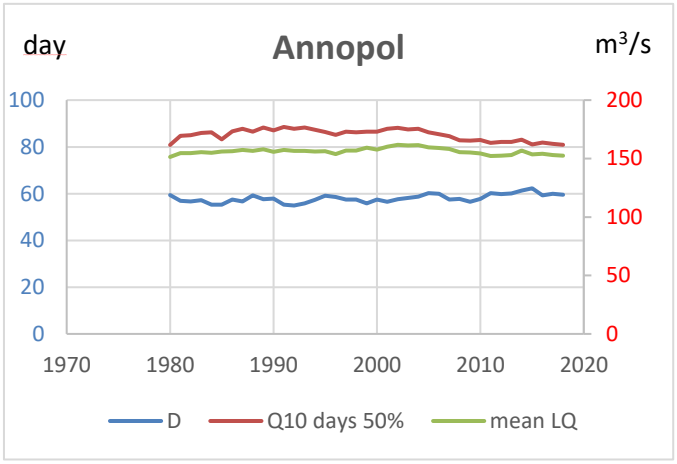

Fig. 3. Design characteristics of low flows $Q_{10,50\%}$, mean LQ and *D*.

The calculations were performed for moving window of 30-year data. On the Middle Vistula the course of the *x* and *y* values in the 30-year moving window does not reveal any significant changes in $Q_{10,50\%}$ and *D*.

The chart of mean daily flows for stations on the Vistula shows the period of low flows (Fig. 4).

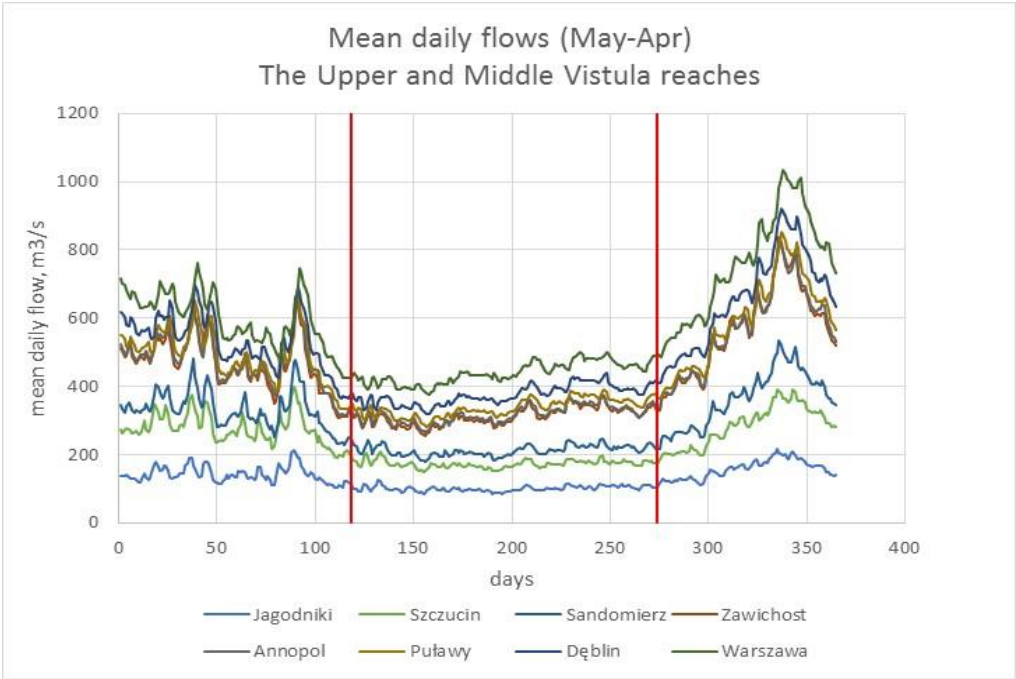

Fig. 4. The potential time period of summer-autumn low flows occurrence for the Upper and Middle Vistula reaches.

The vertical red lines mark the approximate limits: the end of August till the end of January which can be treated as main time of exposure to low flows.

Drought prone areas are difficult to exact designation because in fact the drought can happen everywhere. In this presentation we define the regions of the most probable drought occurrence supporting this decision by hydrologic and human pressures data.

The reliable human activity data are difficult to get and the main problems arise from the fact that national databases identifying all types of pressures are often not spatially referenced. Most of the necessary data are collected, but access to them is difficult or they do not cover all the period required (Karamuz et al. 2021). However it is possible to use and compare maps of different aspects of pressures on water resources and space distribution of hydrological characteristics important from the point of view of low flows development. Here several maps were analysed and five of them are attached below (Figs. 5–9). They are maps of population density, Gross Domestic Product, water withdraw from groundwater bodies, the map of river network density, and mean annual runoff module.

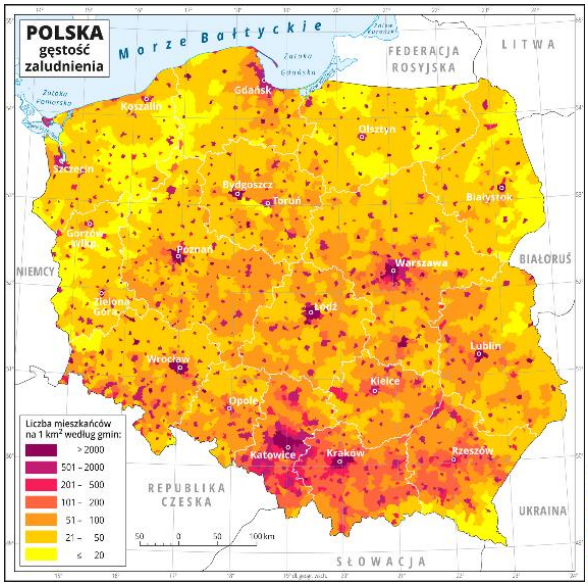

Fig. 5. Population density (persons per 1 km^2 in Poland (by communes).

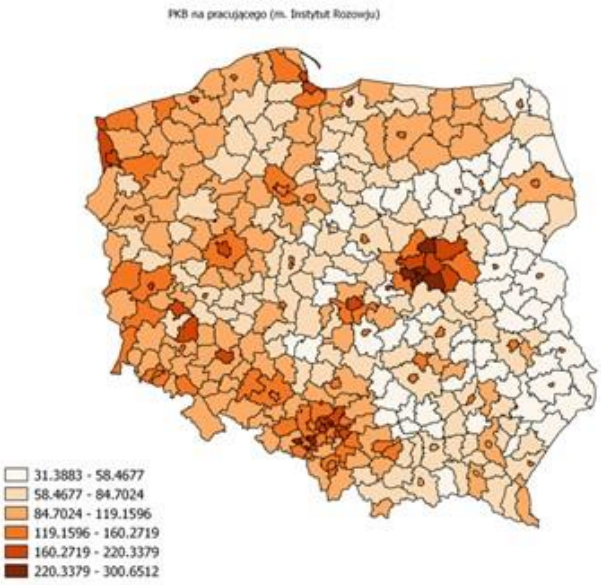

Fig. 6. Gross Domestic Product (GDP) per capita in poviats as a percentage of Total Polish GDP.

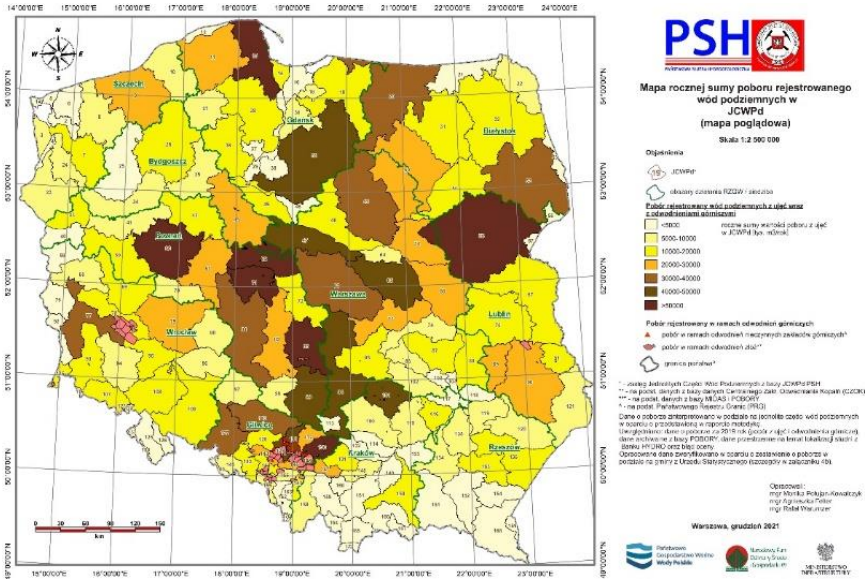

Fig. 7. Annual water withdraw (thousand cubic m/year) from groundwater bodies (colours from light yellow < 500 to darkest brown > 5000).

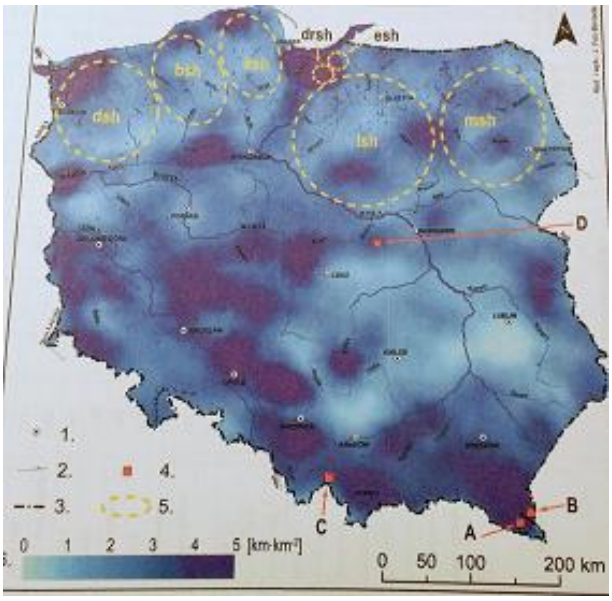

Fig. 8. River network density (km/km^2).

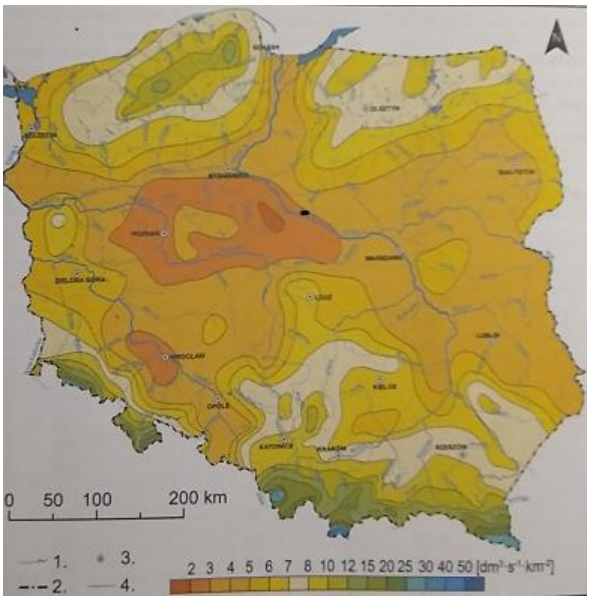

Fig. 9. The runoff module (dm^3 s^{-1} km^{-2}) in Poland.

The visual inspection of this material leads to the conclusion that the most vulnerable to soil and hydrological drought are the areas located in the middle reach of the Vistula especially in Kujawy and Lublin Upland regions. This statement will be made more specific in the future.

Acknowledgments. This work was partially supported within statutory activities No. 3841/E-41/S/2019 of the Ministry of Science and Higher Education of Poland and the project HUMDROUGHT, IG PAS, funded by National Science Centre (contract 2018/30/Q/ST10/00654). The hydro-meteorological data were provided by the Institute of Meteorology and Water Management (IMGW), Poland.

References

Dębski, K. (1967), *Hydrologia*, SGGW, Warszawa (in Polish).

Fal, B. (2007), Niżówki na górnej i środkowej Wiśle, *Gospod. Wodna* **2**, 72–81 (in Polish).

Bogdanowicz, E., E. Karamuz, and R.J. Romanowicz (2021), Temporal changes in flow regime along the River Vistula, *Water* **13**, 20, 2840, DOI: 10.3390/w13202840.

Jokiel, P., W. Marszelewski, and J. Pociask-Karteczka (eds.) (2017), *Hydrologia Polski*, PWN, 341 pp. (in Polish).

Karamuz, E., E. Bogdanowicz, T.B. Senbeta, J.J. Napiórkowski, and R.J. Romanowicz (2021), Is it a drought or only a fluctuation in precipitation patterns?—Drought reconnaissance in Poland, *Water* **13**, 6, 807, DOI: 10.3390/w13060807.

Strupczewski, W.G., and Z. Kaczmarek (2001), Non-stationary approach to at-site flood frequency modelling. Part II. Weighted least squares estimation, *J. Hydrol*. **248**, 1–4, 143–151, DOI: 10.1016/S0022-1694(01)00398-5.

Received 17 November 2022
Accepted 20 December 2022

Publications of the Institute of Geophysics, Polish Academy of Sciences
Geophysical Data Bases, Processing and Instrumentation
vol. 443 (E-13), 2022, pp. 47–54
DOI: 10.25171/InstGeoph_PAS_Publs-2022-042
International Symposium on Drought and Climate Change, 24–25 November 2022

Time Series Clustering using Trend, Seasonal and Autoregressive Components: Patterns of Change of Maximum Temperature in Iberian Peninsula

Arnobio PALACIOS GUTIERREZ[1,2,✉] and Jose Luis VALENCIA DELFA[1]

[1]Complutense University of Madrid, Faculty of Statistical Studies,
Madrid, Community of Madrid, Spain

[2]Technological University of Chocó, Group Valoración y Aprovechamiento de la Biodiversidad,
Quibdó, Chocó-Colombia

✉ arnobiop@ucm.es

Abstract

Time series clustering is an important field of data mining and can be used to identify interesting patterns. This study introduces a new way to obtain clusters of time series by representing them with feature vectors that define the trend, seasonality and noise components of each series, in order to identify areas of the Iberian Peninsula that follow the same pattern of change in their maximum temperature during 1931–2009. Singular spectrum analysis decomposition in a sequential manner is used for dimensionality reduction, which allows the extraction of the trend, seasonality and residual components of each time series corresponding to an area of the Iberian region; then, the feature vectors of the time series are obtained by modelling the extracted components and estimating the parameters. Finally, the series are clustered using a clustering algorithm, and the clusters are defined according to the centroids. The results identified three differentiated zones, allowing to describe how the maximum temperature varied: in the north and central zones, an increase in temperature was noted over time, and in the south, a slight decrease, moreover different seasonal variations were noted according to zones.

Keywords: clustering, maximum temperature time series, singular spectrum analysis, feature vectors of time series, Iberian Peninsula.

1. INTRODUCTION

Climate change is a global problem that has a significant impact on society and ecosystems and is increasingly noticeable. In consequence, studies on climate change have become increasingly more important, especially those relating to temperatures, which have been increasing as stated in the report of the Sixth Assessment of the Intergovernmental Panel on Climate Change (IPCC) that reports that global mean surface temperature (GMST) has increased by 1.1 °C between the 2001–2021 and 1850–1900 periods, after accelerating its rate after the 1970s (IPCC 2021). Moreover, in the very near future, 2020–2050, GMST can warm up as much as 0.25 °C per decade, according to some climate model predictions (Samset et al. 2020; Tebaldi et al. 2021).

Although these numbers may seem low, the changes and effects are really remarkable, as manifested by global warming, prolonged droughts, heat waves and forest fires. In Europe and the Iberian Peninsula (IP) have been experiencing these conditions in the last years (Kuglitsch et al. 2010; Russo et al. 2015; Molina et al. 2020; Calheiros et al. 2021) and according to some climate predictions, is expected these conditions continue for the foreseeable future (IPCC 2014; King and Karoly 2017; Dosio et al. 2018; Vicedo-Cabrera et al. 2018).

Analysis of the temperature changes experienced by the IP, as well as the projections that have arisen around this issue will be a more manageable process if studies that define these changes by zones or sub-regions are include and if analysis that take into account temperature extremes are considered, which tell us about unusual changes (Gebremichael et al. 2022).

A way to define the extreme temperature changes experienced by a geographical area for sub-region is by obtaining time series (TS) clusters of these temperatures defined in points or areas distributed over the geographical area, since; TS clustering is used to identify interesting patterns in TS data sets. There are mainly three categories or approaches to TS clustering (Warren Liao 2005; Rani and Sikka 2012; Aghabozorgi et al. 2015; Ergüner Özkoç 2021), depending on whether they work directly with raw data, indirectly with features or characteristics extracted from the raw data, or indirectly with models built from raw data.

This study is framed within the clustering of TS based on the approach of extracting features from data and proposes a procedure to cluster TS by their trend, seasonality, and main autocorrelations, so that patterns of change in maximum temperature (TMAX) can be identified for zone in the IP during the period 1931–2009. The novelty of our methodology is the use the decomposition of TS using singular spectrum analysis (SSA). In this decomposition process, three components associated with the trend, seasonality and residual of the initial TS are reconstructed, allowing the extraction of the parameters that describe these components. Secondly, the representation of each TS is obtained from a feature vector generated on the basis of the calculated parameters, which allows clustering the TS using unsupervised learning algorithms, such as k-means (Hartigan and Wong 1979), C-medoids (Park and Jun 2009), hierarchical agglomerative (HA) (Lukasová 1979), and Kohonen self-organising maps (SOM) (Kohonen et al. 1996), which are known and representative conventional algorithms that use the Euclidean distance. Finally, in our experiment on a climatic database, after comparing the clusters obtained with the different methods, a hybrid approach that combines HA and k-means, called hkmeans (Lee et al. 2010; Kassambara 2017), is selected as a clustering algorithm to define TS that are similar and follow a pattern. The results made it possible to identify three differentiated zones according to their TMAX level and trend. In addition, was observed that the identified zones show different seasonal variations.

The remainder of this document is organised as follows. Section 2 describes the TS decomposition method using SSA in a sequential manner. Section 3 proposes the new method for defining the trend, seasonality and autoregression patterns of TS. Section 4 presents the results of the method. Section 5 presents the main conclusions of the paper.

2. SEQUENTIAL SSA DECOMPOSITION METHOD

This technique is based on the singular value decomposition (SVD) of a specific matrix obtained from a TS and aims to decompose an original TS into a sum of a small number of interpretable components, such as the trend that is smooth and slowly varying, oscillatory components that are periodic or pure quasiperiodic or amplitude-modulated, and noise without any pattern or structure (Golyandina et al. 2001; Golyandina and Korobeynikov 2014).

In the following, the SSA method is presented formally.

Input: $\mathbb{T} = (\boldsymbol{t_1}, \boldsymbol{t_2}, \ldots, \boldsymbol{t_N})$ the initial TS, which is one-dimensional N-order TS.

Result: A decomposition of $\mathbb{T}$ into a sum of identifiable components $\mathbb{T} = \widetilde{\mathbb{T}}_1 + \widetilde{\mathbb{T}}_2 + \ldots + \widetilde{\mathbb{T}}_m$.

Step 1: **Embedding**. The so-called "trajectory matrix" is obtained as $\boldsymbol{X} = \boldsymbol{\mathcal{T}}(\mathbb{T})$, where $\boldsymbol{\mathcal{T}}$ is a linear map that transforms the TS $\mathbb{T}$ into a matrix of order $L \times K$, where L is an integer that is called the "window length", $1 < L < N$, and $K = \boldsymbol{N} - \boldsymbol{L} + \boldsymbol{1}$.

The set of all possible path matrices can be denoted as $\mathcal{M}_{L,K}^{(\mathcal{H})}$. $\mathcal{H}$ / denotes Hankel matrices, where all elements along the diagonal are equal. If N and L are fixed, then there is a biunivocal correspondence between the path matrices and the TS.

The trajectory matrix $\boldsymbol{X}$ constructed from lagged vectors generated from the TS $\mathbb{T}$ can be represented as:

$$\boldsymbol{\mathcal{T}}(\mathbb{T}) = \begin{pmatrix} \boldsymbol{t_1} & \boldsymbol{t_2} & \boldsymbol{t_3} & & \boldsymbol{t_K} \\ \boldsymbol{t_2} & \boldsymbol{t_3} & \boldsymbol{t_4} & \cdots & \boldsymbol{t_{K+1}} \\ \boldsymbol{t_3} & \boldsymbol{t_4} & \boldsymbol{t_5} & & \boldsymbol{t_{K+2}} \\ & \vdots & & \ddots & \vdots \\ \boldsymbol{t_L} & \boldsymbol{t_{L+1}} & \boldsymbol{t_{L+2}} & \cdots & \boldsymbol{t_N} \end{pmatrix}. \tag{1}$$

Step 2: **Decomposition of $\boldsymbol{X}$ into a sum of the matrices of rank 1.** The result obtained in this step is the decomposition:

$$\boldsymbol{X} = \sum_{\boldsymbol{i}} \boldsymbol{X_i}, \qquad \boldsymbol{X}_i = \sigma_i U_i V_i^T, \tag{2}$$

where $U_i \in R^L$ and $V_i \in R^K$ are vectors such that $\|U_i\| = 1$ and $\|V_i\| = 1$ for all i and σ_i denotes nonnegative numbers.

If such a decomposition is performed by conventional SVD, the corresponding SSA method is "Basic SSA", and the singular value decomposition of the matrix $\boldsymbol{X}$ is calculated via the eigenvalues and eigenvectors of the matrix $S = \boldsymbol{X}\boldsymbol{X}^{\boldsymbol{T}}$ of size $L \times L$. Here, $\lambda_1, \ldots, \lambda_L$ denotes the eigenvalues of the matrix S taken in decreasing order of magnitude ($\lambda_1 \geq \ldots \geq \lambda_L \geq 0$) and $U_i, \ldots, U_L$ denotes the orthonormal system of the eigenvectors of the matrix S corresponding to these eigenvalues. If $d = \text{rank}(\boldsymbol{X}) = \boldsymbol{\max}\{\boldsymbol{i}, \text{ such that } \lambda_i \geq 0\}$ and $V_i = \boldsymbol{X}^{\boldsymbol{T}} U_i / \sqrt{\lambda_i}, (i = 1, \ldots, d)$ are factor vectors, then $\boldsymbol{X}_i = \sqrt{\lambda_i} U_i V_i^T$ are matrices of rank 1, so they are elementary matrices. Thus, the SVD of the trajectory matrix can be written as:

$$\boldsymbol{X} = \boldsymbol{X}_1 + \ldots + \boldsymbol{X}_d \ . \tag{3}$$

The collection $(\sqrt{\lambda_i}, U_i, V_i^T)$ is called an SVD eigenvector of order i and consists of the singular value $= \sqrt{\lambda \sigma_{i_i}}$, an eigenvector U_i (the left singular vector) and a factor vector V_i (the right singular vector).

Step 3: **Grouping.** The input of this step is expansion (2) and a specification of how to cluster the components of Eq. (2). The index set $I = \{1,2, \ldots, d\}$ must be segmented into m disjoint

subsets. $I_1, I_2, \ldots, I_m$. Let $I = \{i_1, i_2 \ldots, i_p\} \subset \{1,2, \ldots, d\}$ be a subset of indices; then, the resulting matrix $\boldsymbol{X}_I$ corresponding to the group I is defined as:

$$\boldsymbol{X}_I = \boldsymbol{X}_{i1} + \boldsymbol{X}_{i2} + \ldots + \boldsymbol{X}_{ip} \ . \tag{4}$$

Thus, if a partition is specified in m disjoint subsets of the index set $\{1,2, \ldots, d\}$, then, by expansion (2), the result of the grouping step leads to the following decomposition:

$$\boldsymbol{X} = \boldsymbol{X}_{I1} + \boldsymbol{X}_{I2} + \ldots + \boldsymbol{X}_{Im} \ . \tag{5}$$

The above procedure for choosing the sets $I_1, I_2, \ldots, I_m$ is called the "eigentriple grouping" procedure. The grouping of expansion (2), where $I_k = \{k\}$, is called "elementary".

Step 4: **Reconstruction**. In this step, each matrix $\boldsymbol{X}_{Ik}$ from lumped decomposition (5) is transferred into the form of the input object $\mathbb{T}$, which is a TS of length N. Such a transformation is optimally performed as follows: Let $\boldsymbol{Y} \in R^{L \times K}$ be a matrix with elements y_{ij}, $1 \le i \le L, 1 \le j \le K$; we look for an object $\widetilde{\mathbb{Y}} \in \mathcal{M}$ that provides the minimum of $\|\boldsymbol{Y} - \boldsymbol{\mathcal{T}}(\mathbb{Y})\|_F$, where $\|\boldsymbol{Z}\|_F = (\sum_{ij} |z_{ij}|^2)^{1/2}$ is the Frobenius norm of $\boldsymbol{Z} = [z_{ij}] \in R^{L \times K}$.

Let $\Pi_{\mathcal{H}} : R^{L \times K} \to \mathcal{M}_{L,K}^{(\mathcal{H})}$ be the orthogonal projection of $R^{L \times K}$ onto $\mathcal{M}_{L,K}^{(\mathcal{H})}$ in the Frobenius norm. Then, $\widetilde{\mathbb{Y}} = \boldsymbol{\mathcal{T}}^{-1} \circ \Pi_{\mathcal{H}}(\boldsymbol{Y})$. The projection $\Pi_{\mathcal{H}}$ is simply the average of the entries corresponding to a given element of an object (Golyandina et al. 2018; Section 1.1.2.6). In Basic SSA, the composite mapping $\boldsymbol{\mathcal{T}}^{-1} \circ \Pi_{\mathcal{H}}$ uses the long average of antidiagonals so that $\tilde{y}_k = \sum_{(i,j) \in \mathcal{A}_k} (\boldsymbol{Y}_{ij}) \ / \ |\mathcal{A}_k|$, where $\mathcal{A}_k = \{(i,j) : i + j = k + 1, 1 \le i \le L, 1 \le j \le K\}$.

If $\widehat{\boldsymbol{X}}_k = \boldsymbol{X}_{Ik}$ are the reconstructed matrices, $\widetilde{\boldsymbol{X}}_k = \Pi_{\mathcal{H}} \widehat{\boldsymbol{X}}_k$ are their corresponding path matrices, and $\widetilde{\mathbb{T}}_k = \boldsymbol{\mathcal{T}}^{-1}(\widetilde{\boldsymbol{X}}_k)$ are the reconstructed objects. Then, the resulting decomposition of the input object $\mathbb{T}$ is:

$$\mathbb{T} = \widetilde{\mathbb{T}}_1 + \widetilde{\mathbb{T}}_2 + \ldots + \widetilde{\mathbb{T}}_m \ . \tag{6}$$

If the grouping is elementary, the reconstructed objects $\widetilde{\mathbb{T}}_k$ in Eq. (6) are called "elementary components".

The SSA parameters, i.e., length of the window L and the way in which $\boldsymbol{X}_{ik}$ matrices are grouped, are very important for the outcome of the decomposition and depend on properties of the initial TS and the objective of the analysis, check Golyandina et al. (2001) for more details.

SSA can be performed sequentially, which is recommended when the TS structure is complex (Golyandina et al. 2012). ***Sequential SSA*** consists of two stages: the first stage performs the extraction of the TS trend with a small L, and in the second stage, the periodic components of the residue are detected and extracted with $L \sim N \ / \ 2$.

3. TREND, SEASONALITY AND AUTOREGRESSION SSA-BASED TS PATTERN IDENTIFICATION

The algorithm for the identification of trend, seasonality and autoregression patterns in TS proposed in this study can be summarised in the following steps:

1) Perform sequential SSA to extract the 3 components of the initial TS associated with the trend, seasonality and residual part.
2) Model the extracted TS in such a way that their associated characteristics can be extracted:
    a. Trend component: from $\mathbb{T}_{\text{trend}} = \mu - \beta t$, estimate μ and β;

b. Seasonal component: from $\mathbb{T}_{\text{seasonal}} = c_1 \sin(2\pi t/T) + c_2 \cos(2\pi t/T)$, where T is the period, estimate c_1 and c_2;
c. Residual part: from $\mathbb{T}_{\text{residual}}$, obtain an $AR(T)$ and calculate the autocorrelations $\varphi_1, \varphi_2, \varphi_3$, and φ_s, where $s = T$, the period.

A feature vector is constructed for each initial TS by considering the estimated parameters.

3) Use a conventional algorithm to obtain a similar TS.
4) By averaging the initial TS of each group, the representative patterns of each group are obtained based on the defined characteristics.

4. RESULTS AND ANALYSIS

A set of 1776 points from a grid of 25 × 25 km^2 elaborated through spatial interpolation kriging by the "Servicio de Desarrollos Climatológicos" of the Meteorological Spanish State Agency was used. This grid includes points distributed in Spain, Portugal and the closest areas of the Atlantic Ocean and the Mediterranean Sea, for each point a monthly TS of TMAX from January 1931 to 2009 is considered.

After comparing the four clustering algorithms, k-means, k-medoids, HA and SOM, on the dataset, given the superiority of HA and K-Means, a hybrid method, called hierarchical k-means (hkmeans), was selected.

Here, hkmeans is applied to the set formed by the feature vectors of the TS. The results are shown in Fig. 1.

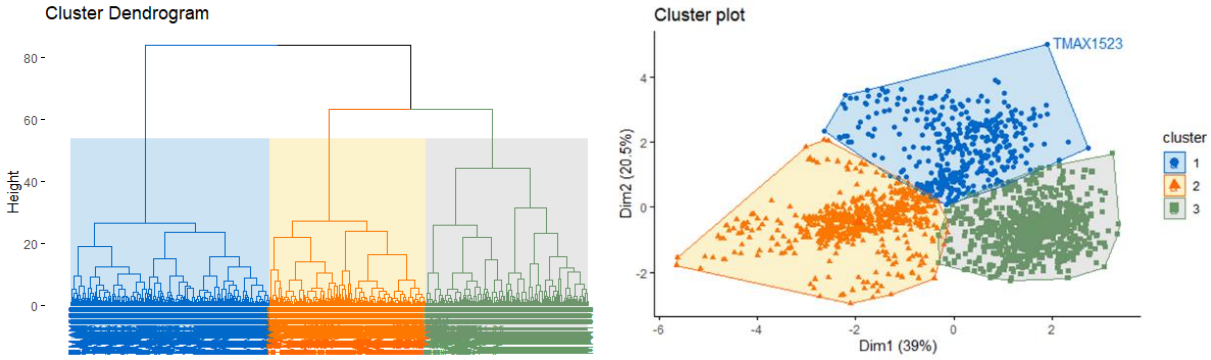

Fig. 1. Result of the hkmeans cluster.

Figure 2 illustrates the distribution (the grid is composed of longitudes and latitudes in UTM coordinates) of the points in Spain according to the clusters obtained.

Clearly, three clusters can be observed; zone 1 situated in the north of the IP, where the areas with the lowest TMAX and with a higher proportion of increase compared to the other areas are found, zone 2, more to the south, where the areas with the highest TMAX are located, but showing a slight decline over the period, and zone 3, with areas more towards the centre and with intermediate TMAX, which also show an increase over time. In addition, was observed that the identified zones show different seasonal variations.

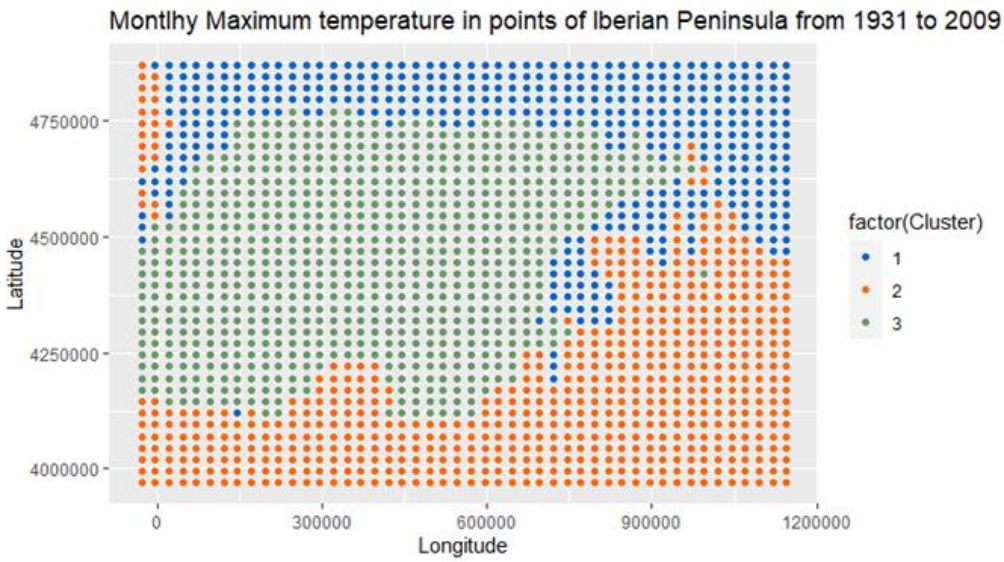

Fig. 2. Distribution of points in Spain according to geographical location and clusters.

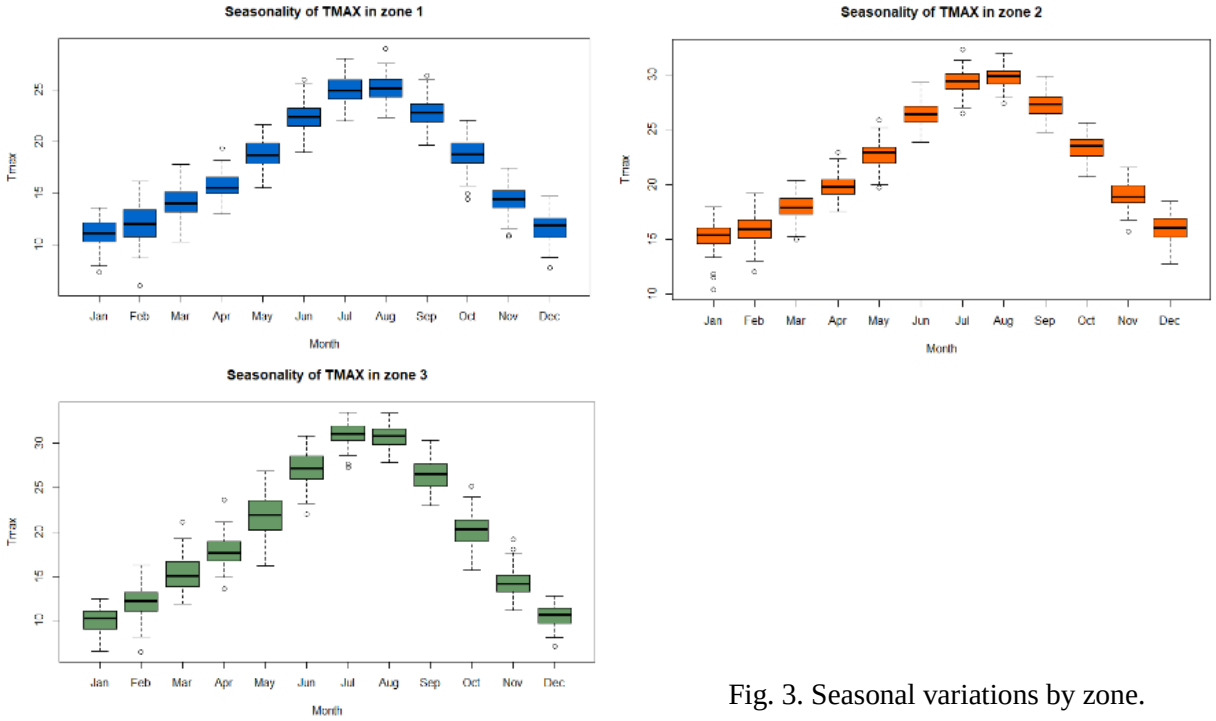

Fig. 3. Seasonal variations by zone.

Figure 3 shows the seasonal variations by zone. It can be noted that, zone 1 shows its largest variations in winter months and, zone 3, in spring and autumn months. Zone 2 does not show marked differences in its monthly variation.

5. CONCLUSIONS

In this paper, we present a new method for clustering TS by taking into account their trend, seasonality, and residual components. The procedure allowed to describe how the maximum temperature varied in the Iberian Peninsula during 1931–2009 through three zones defined according to their trend and monthly variation. The north of the Iberian Peninsula, where the

areas with the lowest maximum temperatures are found, experienced a 0.2034°C increase in its maximum temperature per decade between 1931 and 2009, the south, where the areas with the highest maximum temperatures are located, only showed a slight decline, and the central zone, showed an increase of 0.135°C per decade.

Acknowledgments. We express our gratitude to "Servicio de Desarrollos Climatológicos" of the Meteorological Spanish State Agency for providing the data used in the study, and the Colombian Ministry of Science for the support in the doctoral formation of Arnobio Palacios.

References

Aghabozorgi, S., A. Seyed Shirkhorshidi, and T. Ying Wah (2015), Time-series clustering – A decade review, *Inform. Syst.* **53**, 16–38, DOI: 10.1016/j.is.2015.04.007.

Calheiros, T., M.G. Pereira, and J.P. Nunes (2021), Assessing impacts of future climate change on extreme fire weather and pyro-regions in Iberian Peninsula, *Sci. Total Environ.* **754**, 142233, DOI: 10.1016/j.scitotenv.2020.142233.

Dosio, A., L. Mentaschi, E.M. Fischer, and K. Wyser (2018), Extreme heat waves under 1.5 °C and 2 °C global warming, *Environ. Res. Lett.* **13**, 5, 054006, DOI: 10.1088/1748-9326/aab827.

Ergüner Özkoç, E. (2021), Clustering of time-series data. **In:** D. Birant (ed.), *Data Mining – Methods, Applications and Systems*, IntechOpen, London, 87–106, DOI: 10.5772/intechopen.84490.

Gebremichael, H.B., G.A. Raba, K.T. Beketie, G.L. Feyisa, and T. Siyoum (2022), Changes in daily rainfall and temperature extremes of upper Awash Basin, Ethiopia, *Sci. Afr.* **16**, e01173, DOI: 10.1016/j.sciaf.2022.e01173.

Golyandina, N., and A. Korobeynikov (2014), Basic Singular Spectrum Analysis and forecasting with R, *Comput. Stat. Data An.* **71**, 934–954, DOI: 10.1016/j.csda.2013.04.009.

Golyandina, N., A. Pepelyshev, and A. Steland (2012), New approaches to nonparametric density estimation and selection of smoothing parameters, *Comput. Stat. Data An.* **56**, 7, 2206–2218, DOI: 10.1016/j.csda.2011.12.019.

Golyandina, N., A. Korobeynikov, and A. Zhigljavsky (2018), *Singular Spectrum Analysis with R*, Springer-Verlag, Berlin, DOI: 10.1007/978-3-662-57380-8.

Golyandina, N., V. Nekrutkin, and A.A. Zhigljavsky (2001), *Analysis of Time Series Structure: SSA and Related Techniques*, Monographs on Statistics and Applied Probability, Vol. 90, Chapman & Hall/CRC, Boca Raton, 320 pp.

Hartigan, J.A., and M.A. Wong (1979), Algorithm AS 136: A K-Means Clustering Algorithm, *J. Roy. Stat. Soc. C: Appl. Statist.* **28**, 1, 100–108, DOI: 10.2307/2346830.

IPCC (2014), *Climate Change 2014: Synthesis Report. Contribution of Working Groups I, II and III to the Fifth Assessment Report of the Intergovernmental Panel on Climate Change*, IPCC, Geneva, Switzerland, 151 pp.

IPCC (2021), *Climate Change 2021: The Physical Science Basis. Contribution of Working Group I to the Sixth Assessment Report of the Intergovernmental Panel on Climate Change* (V. Masson-Delmotte et al. (eds.)), Intergovernmental Panel on Climate Change, available from: https://www.ipcc.ch/report/ar6/wg1/downloads/report/IPCC_AR6_WGI_FrontMatter.pdfwww.ipcc.ch.

Kassambara, A. (2017), *Practical Guide To Cluster Analysis in R. Unsupervised Machine Learning*, Multivariate Analysis, Vol. 1, STHDA, 187 pp.

King, A.D., and D.J. Karoly (2017), Climate extremes in Europe at 1.5 and 2 degrees of global warming, *Environ. Res. Lett.* **12**, 11, 114031, DOI: 10.1088/1748-9326/aa8e2c.

Kohonen, T., E. Oja, O. Simula, A. Visa, and J. Kangas (1996), Engineering applications of the self-organizing map, *Proc. IEEE* **84**, 10, 1358–1384, DOI: 10.1109/5.537105.

Kuglitsch, F.G., A. Toreti, E. Xoplaki, P.M. Della-Marta, C.S. Zerefos, M. Türkeş, and J. Luterbacher (2010), Heat wave changes in the eastern Mediterranean since 1960, *Geophys. Res. Lett.* **37**, 4, L04802, DOI: 10.1029/2009GL041841.

Lee, A.J.T., M.C. Lin, R.T. Kao, and K.T. Chen (2010), An effective clustering approach to stock market prediction, *PACIS 2010 Proceedings* **54**, 345–354, available from: https://aisel.aisnet.org/pacis2010/54.

Lukasová, A. (1979), Hierarchical agglomerative clustering procedure, *Pattern Recogn.* **11**, 5–6, 365–381, DOI: 10.1016/0031-3203(79)90049-9.

Molina, M.O., E. Sánchez, and C. Gutiérrez (2020), Future heat waves over the Mediterranean from an Euro-CORDEX regional climate model ensemble, *Sci. Rep.* **10**, 1, 8801, DOI: 10.1038/s41598-020-65663-0.

Park, H.S., and C.H. Jun (2009), A simple and fast algorithm for K-medoids clustering, *Expert Syst. Appl.* **36**, 2, part 2, 3336–3341, DOI: 10.1016/J.ESWA.2008.01.039.

Rani, S., and G. Sikka (2012), Recent techniques of clustering of time series data: A survey, *Int. J. Comput. Appl.* **52**, 15, 1–9, DOI: 10.5120/8282-1278.

Russo, S., J. Sillmann, and E.M. Fischer (2015), Top ten European heatwaves since 1950 and their occurrence in the coming decades, *Environ. Res. Lett.* **10**, 12, 124003. DOI: 10.1088/1748-9326/10/12/124003.

Samset, B.H., J.S. Fuglestvedt, and M.T. Lund (2020), Delayed emergence of a global temperature response after emission mitigation, *Nat. Commun.* **11**, 1, 3261, DOI: 10.1038/s41467-020-17001-1.

Tebaldi, C., K. Debeire, V. Eyring, E. Fischer, J. Fyfe, P. Friedlingstein, R. Knutti, J. Lowe, B. O'Neill, B. Sanderson, D. van Vuuren, K. Riahi, M. Meinshausen, Z. Nicholls, K.B. Tokarska, G. Hurtt, E. Kriegler, J.-F. Lamarque, G. Meehl, et al. (2021), Climate model projections from the Scenario Model Intercomparison Project (ScenarioMIP) of CMIP6, *Earth Syst. Dynam.* **12**, 1, 253–293, DOI: 10.5194/esd-12-253-2021.

Vicedo-Cabrera, A.M., Y. Guo, F. Sera, V. Huber, C.-F. Schleussner, D. Mitchell, S. Tong, M. de S.Z.S. Coelho, P.H.N. Saldiva, E. Lavigne, P.M. Correa, N.V. Ortega, H. Kan, S. Osorio, J. Kyselý, A. Urban, J.J.K. Jaakkola, N.R.I. Ryti, M. Pascal, et al. (2018), Temperature-related mortality impacts under and beyond Paris Agreement climate change scenarios, *Climatic Change* **150**, 3–4, 391–402, DOI: 10.1007/s10584-018-2274-3.

Warren Liao, T. (2005), Clustering of time series data – A survey, *Pattern Recogn.* **38**, 11, 1857–1874, DOI: 10.1016/j.patcog.2005.01.025.

Received 17 November 2022
Accepted 20 December 2022

Publications of the Institute of Geophysics, Polish Academy of Sciences
Geophysical Data Bases, Processing and Instrumentation
vol. 443 (E-13), 2022, pp. 55–58
DOI: 10.25171/InstGeoph_PAS_Publs-2022-043
International Symposium on Drought and Climate Change, 24–25 November 2022

Understanding the Temporal and Spatial Dimensions of Socio-hydrological Vulnerability to Drought in the Context of Climate Change, Vistula River

Tesfaye SENBETA✉, Emilia KARAMUZ, Krzysztof KOCHANEK,
and Jarosław NAPIÓRKOWSKI

Department of Hydrology and Hydrodynamics, Institute of Geophysics,
Polish Academy of Sciences, Warsaw, Poland

✉ tsenbeta@igf.edu.pl

A b s t r a c t

In the Anthropocene, droughts cannot be considered as natural phenomena/ hazards. Therefore, it became crucial to assume human impacts and their interactions with the water system in drought vulnerability assessment through the concept of the socio-hydrology. We applied the socio-hydrological approach for identifying drought-vulnerable areas in the Vistula River basin. The Soil and Water Assessment Tool (SWAT) model was used to derive missing hydro-climatic variables, such as soil moisture at sub-basins and hydrological response unit level. The vulnerability indicator was selected based on the statistical significance of the factors affecting the water resources and socio-economics of the drought-prone. The preliminary results showed that the middle part of the Vistula catchment is more exposed to drought than the upper and lower parts of the main river course.

Keywords: drought vulnerability, socio-hydrology, SWAT model, Vistula River basin, vulnerability indicators.

1. INTRODUCTION

One of the droughts definitions often considers it as a climatic phenomenon triggered by a precipitation deficits alone. However, in the Anthropocene when human activities strongly influence the Earth's system, anthropogenic activities also play an important role in influencing drought dynamics. Therefore, the new concept of socio-hydrological approach has been pro-

posed in hydrology to consider the impact of humans and their interactions with the water system (Boori and Voženílek 2014). This new approach is used to assess the dynamics of drought vulnerability over time and space based on an integrated approach that considers multiple factors, including physiographic, social, and hydroclimatic factors. The factors are selected according to their impact, data availability, and reliability out of the three basic dimensions of socio-hydrological vulnerability: (i) Exposure, (ii) Sensitivity, and (iii) Adaptive Capacity. Previous studies on drought vulnerability focused on physiographic and hydro-climatic factors (e.g., Jain et al. 2015; Pandey et al. 2010; Singh et al. 2019) and to our knowledge only few studies considered socio-economic factors, especially people's coping capacity, in assessing drought vulnerability. The aim of this study is, therefore, to assess and identify social and physical vulnerability to drought through the socio-hydrological approach. The novelty of this study is the integration of several hydro-climatic drought indicators as a single index in socio-hydrological vulnerability mapping using marginal likelihood function. This will help with the identification of the areas vulnerable to drought risks and support a drought prevention and climate change adaptation.

2. DATA AND METHODS

2.1 Study area

The study area consists of six sub-basins in the Vistula River basin (Fig. 1). These sub-basins were selected to reflect hydrological conditions caused by significant change in runoff due to human impacts. The predominant land use in the Vistula River basin is agriculture, followed by forest and semi-natural areas. The most severe and longest-lasting drought in the catchment occurred in 1982–1993 (Karamuz et al. 2021). The long-term average hydroclimatic variables varies spatially across the basin, with the highest values occurring near the headwaters and the lowest in the middle part (Senbeta et al. 2022).

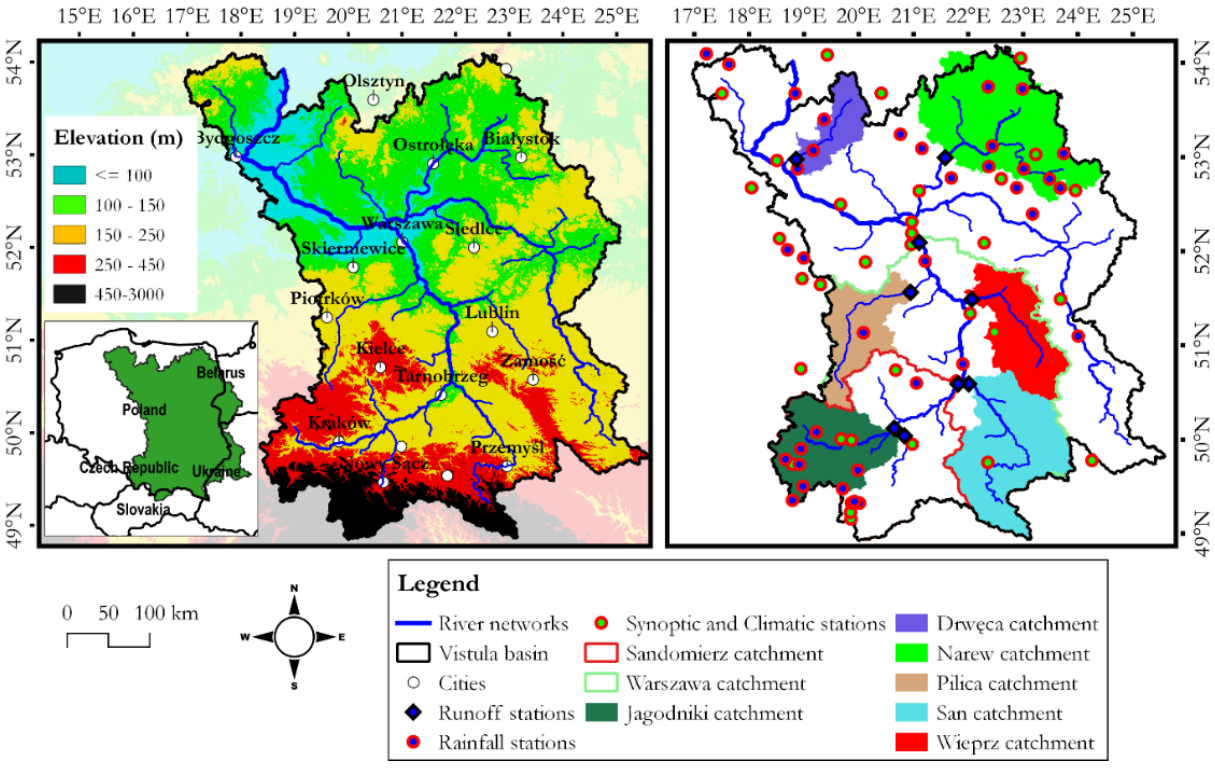

Fig. 1. The location of the Vistula River basin with topographical features (left panel), six selected sub-basins and their hydroclimatic variables (right panel) (Senbeta et al. 2022).

2.2 Methodology

The Drought Vulnerability Index (DVI) was proposed based on vulnerability factors selected considering the three vulnerability dimensions (exposure, sensitivity, and coping capacity) in an integrated perspective. The geophysical, hydroclimatic, and socio-economic data for the study area were collected from the relevant authorities in Poland and worldwide database, while others were prepared by means of Geographical Information System (GIS) using remote-sensing data. The vulnerability indicators were considered in drought vulnerability assessment if the proposed indicator significantly affect the social and hydrological conditions of areas (Boori and Voženílek 2014). Each indicator was firstly standardised and used to determine the DVI using balanced weighting scheme. The Soil and Water Assessment Tool (SWAT) was applied to derive the hydroclimatic variables for sub-basins where measurements were not available.

3. PRELIMINARY RESULTS

In the last 7 decades, the Vistula River basin has experienced several droughts. For example, majority of the basin was affected by the drought events of the 1980s which varied in terms of the severity, spatial extent, and duration of occurrence. The sub-basins in the middle of the Vistula River basin (Rivers Pilica and Wieprz) were affected stronger in terms of exposure than the sub-basins in the upper and lower basin (Fig. 2). However, vulnerability to drought varies within the basin when considering the three dimensions (E, S, and AC). Shallow aquifer in the sub-basins near the outflow feeds the runoff during drought, which could help to reduce the vulnerability of the areas (Fig. 3). The potential evapotranspiration had been declining until the early 1980s and then steadily increasing, similar to temperature, as a result of climate change. This could increase the impact of droughts on water availability and vulnerability, unless policy-makers introduce sustainable water resource management that takes climate change into account in the future.

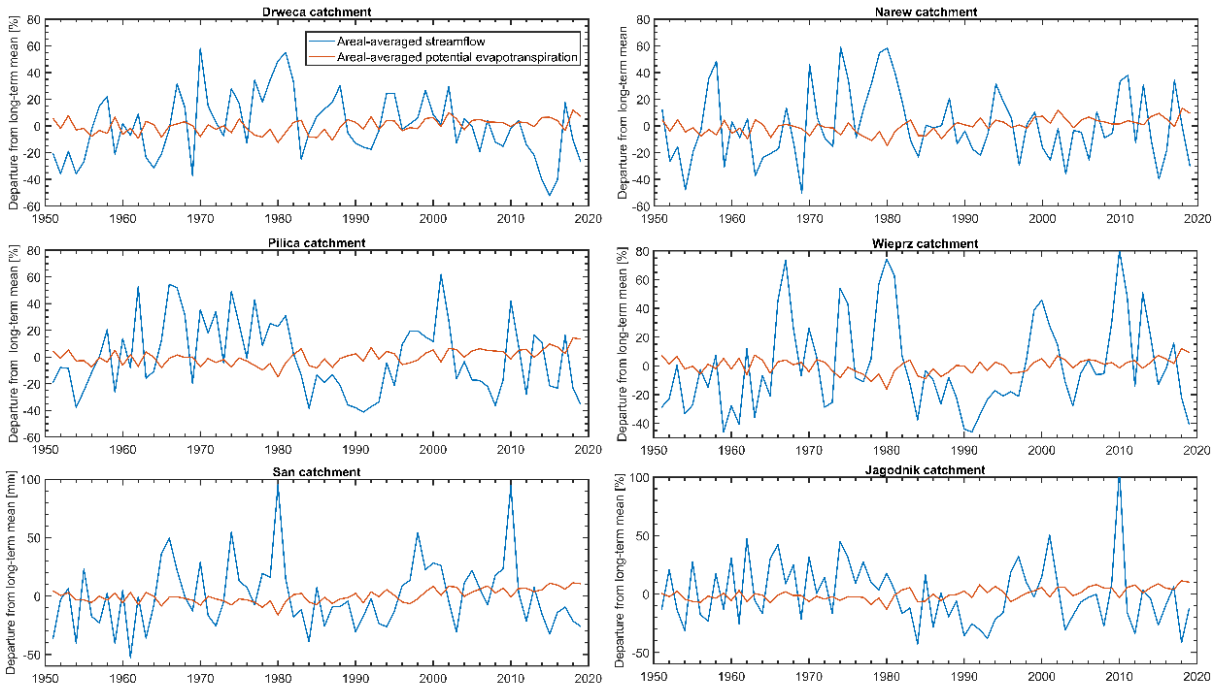

Fig. 2. Annual departure in streamflow and potential evapotranspiration from the long-term mean in the study area.

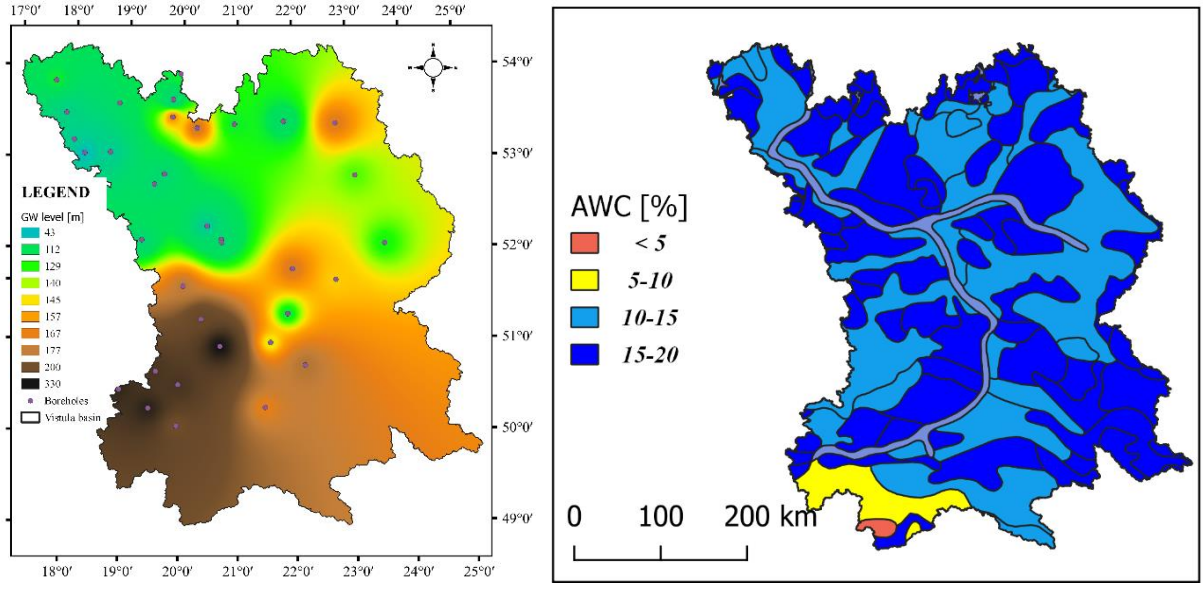

Fig. 3. Long-term average groundwater level (GW) below ground surface and soil available water capacity (AWC) in the Vistula River basin.

Acknowledgments. We express our gratitude to the Institute of Meteorology and Water Management (IMGW) and the Polish Geological Institute (PIG), Poland for providing hydroclimatic and geophysical data. The study was supported by the HUMDROUGHT project funded by the National Science Centre (contract 2018/30/Q/ST10/00654).

References

Boori, M.S., and V. Voženílek (2014), Socio-hydrological vulnerability: A new science through remote sensing and GIS, *Global J. Res. Eng.* **14**, E4, 37–41.

Jain, V.K., R.P. Pandey, and M.K. Jain (2015), Spatio-temporal assessment of vulnerability to drought, *Nat. Hazards* **76**, 1, 443–469, DOI: 10.1007/s11069-014-1502-z.

Karamuz, E., E. Bogdanowicz, T.B. Senbeta, J.J. Napiórkowski, and R.J. Romanowicz (2021), Is It a Drought or Only a Fluctuation in Precipitation Patterns? — Drought Reconnaissance in Poland, *Water* **13**, 6, 807, DOI: 10.3390/w13060807.

Pandey, R.P., A. Pandey, R.V. Galkate, H.R. Byun, and B.C. Mal (2010), Integrating hydro-meteorological and physiographic factors for assessment of vulnerability to drought, *Water Resour. Manage*. **24**, 15, 4199–4217, DOI: 10.1007/s11269-010-9653-5.

Senbeta, T.B., E. Karamuz, K. Kochanek, and J.J. Napiórkowski (2022), Budyko-based approach for modelling water balance dynamics considering environmental change drivers, the River Vistula, Poland (submitted).

Singh, G.R., M.K. Jain, and V. Gupta (2019), Spatiotemporal assessment of drought hazard, vulnerability and risk in the Krishna River basin, India, *Nat. Hazards* **99**, 2, 611–635, DOI: 10.1007/s11069-019-03762-6.

Received 17 November 2022
Accepted 20 December 2022

Publications of the Institute of Geophysics, Polish Academy of Sciences
Geophysical Data Bases, Processing and Instrumentation
vol. 443 (E-13), 2022, pp. 59–63
DOI: 10.25171/InstGeoph_PAS_Publs-2022-044
International Symposium on Drought and Climate Change, 24–25 November 2022

Discrepancies in the Spatial Assessment of Drought – the Vistula Catchment Study

Emilia KARAMUZ✉, Iwona KUPTEL-MARKIEWICZ, Tesfaye SENBETA,
Ewa BOGDANOWICZ, and Jarosław J. NAPIÓRKOWSKI

Institute of Geophysics, Polish Academy of Sciences, Warsaw, Poland
✉ emikar@igf.edu.pl

A b s t r a c t

In the last decade, uncertainty in drought assessment studies has received increasing attention in the hydrometeorological research community. Spatio-temporal characteristics of drought are affected by uncertainties resulting from the calculation of standardized drought indices. To the best of our knowledge, no studies have been conducted so far on the impact of these uncertainties on the assessment of the spatial extent of droughts. In the present study, the uncertainty of determining the spatial extent of meteorological drought in individual classes is investigated for various probability distributions and the accumulation time scale used for determination of the Standardized Precipitation Index (SPI). In the studies, the E-OBS daily gridded precipitation data for the Vistula catchment in Poland were used along with four parametric distribution functions (Birnbaum-Saunders – BS, Weibull – WEI, Generalized Extreme Value – GEV, and Gamma – GAM) and nonparametric approach. Preliminary results indicate significant discrepancies in the spatial extent of individual drought category indicating higher uncertainty in determining the areas affected by severe and extreme droughts.

Keywords: drought, Standardized Precipitation Index, uncertainty analysis, probability distributions.

1. INTRODUCTION

The Standardized Precipitation Index (SPI) is one of the most widely used indicators in drought assessment studies due to its flexibility, spatial-temporal comparability, and quite simple calculation (McKee et al. 1993). Bearing in mind the above advantages, the World Meteorological Organization recommended SPI for meteorological drought assessment, pointing out that SPI allows for a reliable comparison of historical and current droughts between different climatic and geographic regions.

Nevertheless, the SPI is a relative measure. Its calculation depends mainly on the probability density function (PDF) adopted as well as on the method used for parameter estimation and the reference period used in the estimation (Wang et al. 2021). Nowadays, the drought research community focuses on some issues related with applying SPI in different regions. The most questionable is the selection of the adequate probability distribution to fit the cumulative precipitation, the proper time scale, the data length, and the adequacy of the assumption of non-stationarity of the observations.

The proper choice of probability distribution for precipitation is the basis for accurate SPI calculation. The use of different types of distributions lead to different SPI values and may introduce inaccuracies in the assessment of the extent of the impact of the drought phenomenon. In the present study, the uncertainty of meteorological drought extent determination in specific classes is investigated from a candidate probability distribution perspective and the cumulative time scale. The study's main goal was to compare and highlight the discrepancies in determining the spatial extent of drought impacts resulting from using different candidate distributions to calculate SPI.

2. MATERIALS AND METHODS

The SPI was determined for the catchment area of the Vistula River (194 000 km^2), the largest river in Poland (Fig. 1a.). Studied basin is located mainly on the Polish territory and occupies 54% of the country. The study used Europe-wide E-OBS ensemble daily precipitation data set delivered by the European Climate Assessment & Dataset project (ECA&D). The gridded data set covers the period 1950–2020 and has spatial resolution at a spacing of 0.1° × 0.1° in regular latitude/longitude coordinates. The spatial distribution of the long-term (1950–2020) average annual precipitation for the study area is shown in Fig. 1b. The highest yearly average precipitation totals are observed in the southern part of the catchment, where there are mountainous areas. In general, precipitation decreases from south to north, with a clearly distinguishable area of the lowest precipitation in the central part of the catchment.

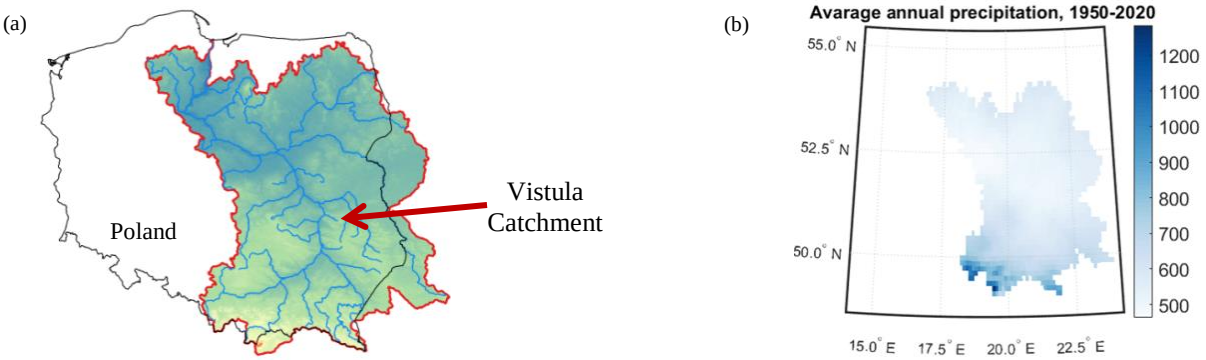

Fig. 1: (a) Study area and (b) spatial distribution of average annual precipitation (1950–2020).

The SPI is calculated as a transformation of one probability distribution (in this case, four probability distributions were used: BS, WEI, GEV, GAM) to the normal distribution using a long-term cumulative precipitation data at a given level of aggregation. Calculation of SPI was done for four aggregation scales, i.e., 1, 3, 6, and 12 months. The goodness-of-fit of the PDF for the E-OBS precipitation data was evaluated based on non-parametric Kolmogorov–Smirnov (KS) test and Akaike Information Criterion (AIC).

3. PRELIMINARY RESULTS

The four PDFs considered were tested for their goodness-of-fit to the precipitation data of different aggregation periods. Figure 2 shows the result of the KS test for the individual PDFs. The pixels highlighted in yellow indicate the regions where the null hypothesis regarding the fit of the proposed PDF cannot be accepted at a significance level of $\alpha = 0.005$, while catchment areas highlighted in dark blue meet the null hypothesis.

The results of the KS test for the GAM and GEV distributions satisfy the null hypothesis for all of the aggregation periods tested and for almost the whole catchment area. The worst performance is for the BS distribution for the 1-month accumulation period. The BS distribution performs comparable to the GEV and GAM distributions for other aggregation scales. The WEI distribution does not meet the null hypothesis for the 3, 6, and 12-monthly accumulation periods for most of the catchment area, and this distribution performs the worst compared to the others.

In the next step, the best-fit distribution was selected using the AIC criterion. The obtained AIC values (Fig. 3) for the individual pixels were averaged over the catchment area. The winning distribution was the one with the lowest AIC value. For the 1-, 3-, and 6-month accumulation period, the GAM distribution was the best choice. For the 12-month time scale, the GEV was the best option.

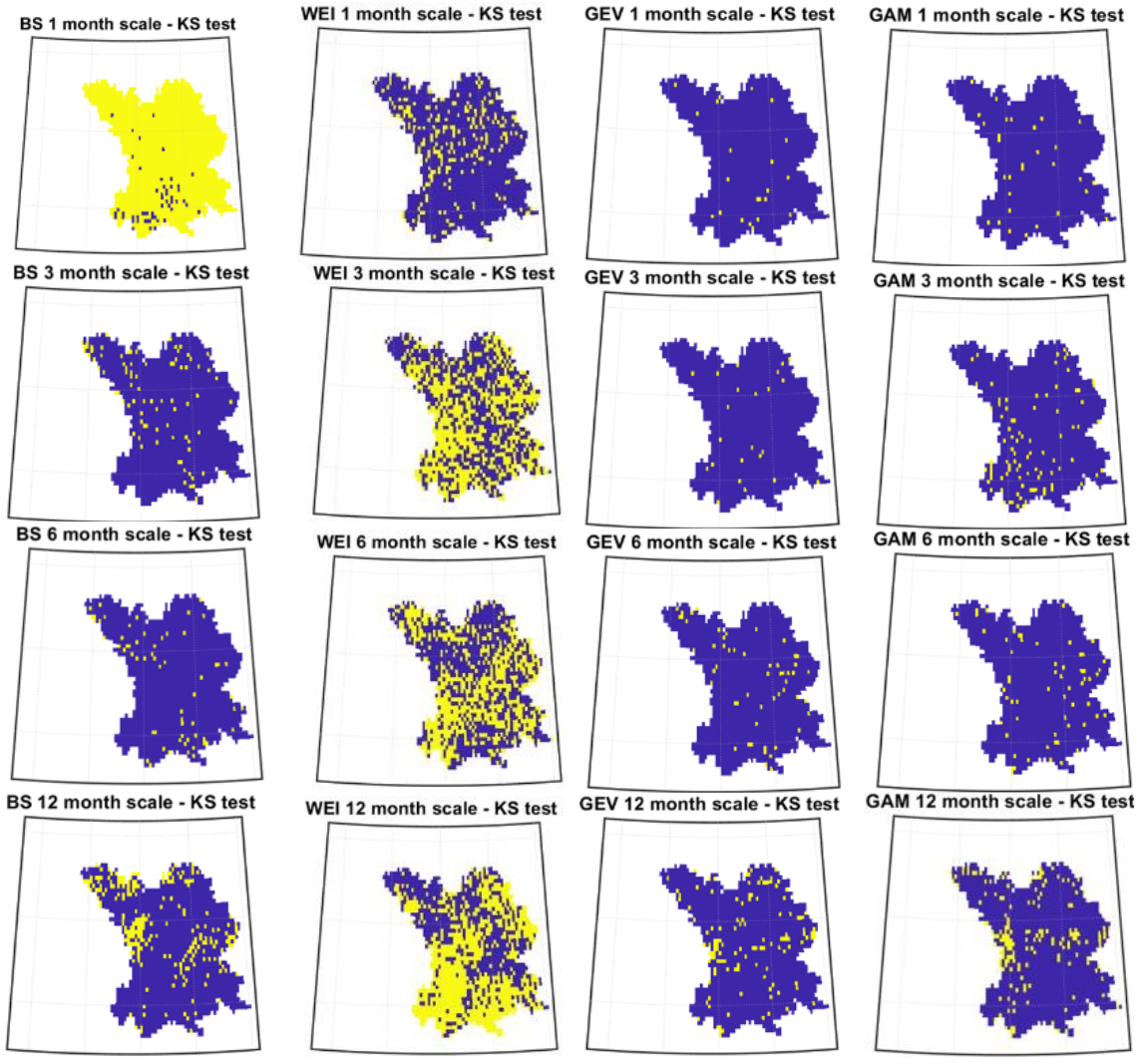

Fig. 2. Results of Kolmogorov–Smirnov test for four candidate PDFs.

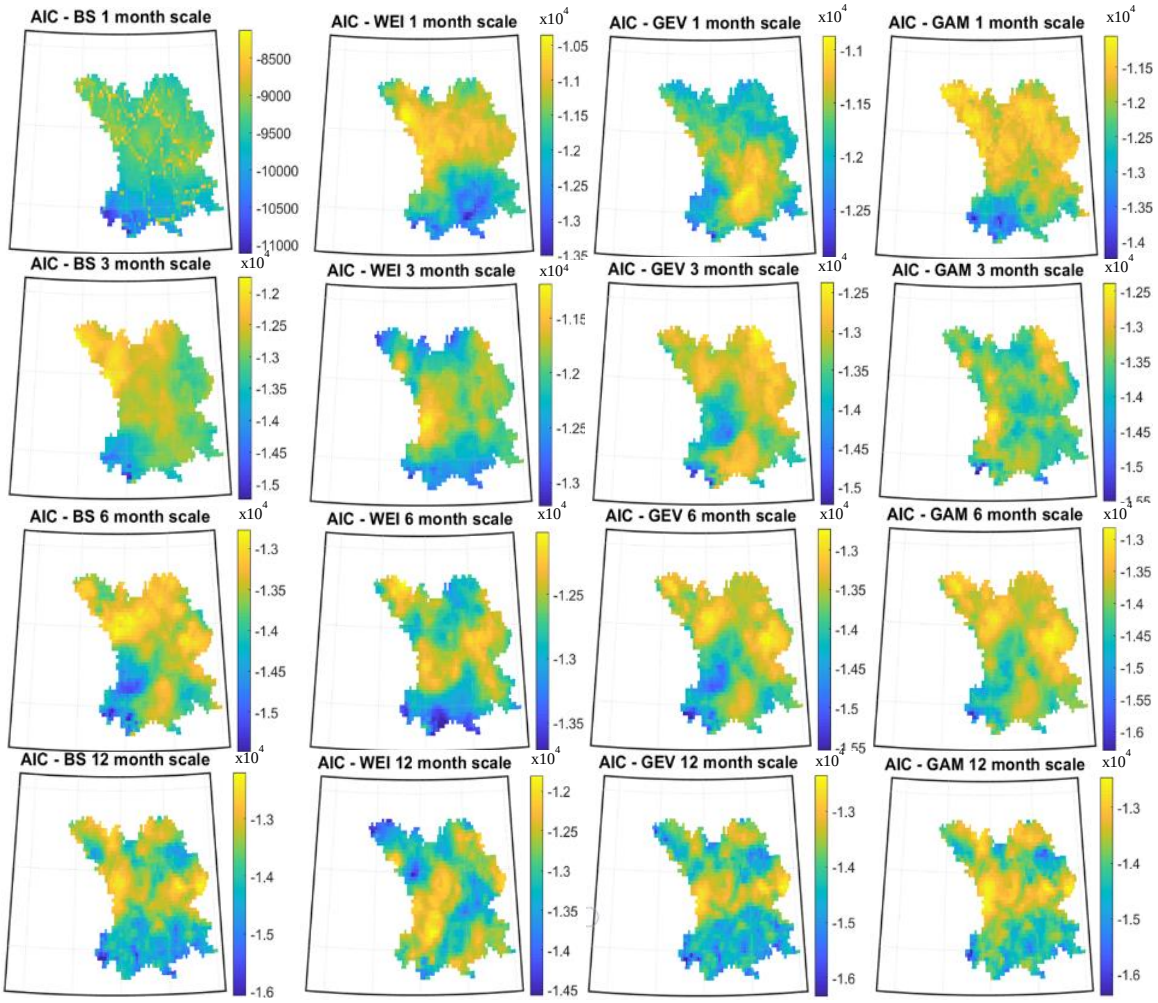

Fig. 3. Goodness-of-fit of four candidate PDFs based on AIC.

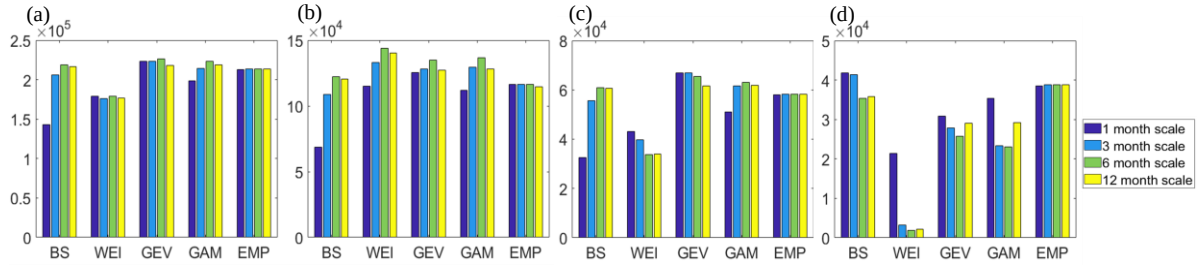

Fig. 4. Number of grid cells classified as: (a) drought – SPI < 0, (b) moderate drought – SPI < –1, (c) severe drought – SPI < –1.5, and (d) extreme drought – SPI < –2.

Finally, to show the quantitative differences in the area classified as a drought event, the SPI values calculated using the proposed distributions were compared (Fig. 4). Nonparametric SPI obtained using the empirical distribution function (EMP) were also presented. They were derived using the Gringorten plotting position approach (Gringorten 1963). The results were shown for different drought categories (moderate, severe, extreme) taking into account different accumulation periods. Analyzing all drought events (SPI < 0), it is evident that variation in their number depends on PDF type used to calculate the drought index. Significant differences can be observed for the WEI distribution for all accumulation periods compared to the other distributions. The WEI distribution tends to underestimate the number of droughts. It is particularly

noticeable for the severe and extreme drought categories (Fig. 1c,d.). For all drought events, the BS distribution underestimates the number of droughts for a 1-month accumulation period. The same regularity is obtained for moderate and severe droughts. The BS distribution stands out in respect to extreme droughts, clearly overestimating the number of droughts (Fig. 1d) compared to other theoretical distributions (especially for the 1- and 3-month accumulation period). Comparing the results with the EMP approach, they are generally consistent to those obtained using the GAM and GEV distributions (Fig. 4a,b,c.). Significant differences occur only for extreme droughts (Fig. 4d). The EMP approach shows high stability of the results for individual accumulation periods, yielding a similar number of drought events for each accumulation period. This regularity is observed for all drought categories. Preliminary results indicate significant discrepancies in the spatial classification of individual drought categories, indicating high uncertainty in determining the area affected by severe and extreme droughts.

Acknowledgments. We express our gratitude to the E-OBS dataset from the EU-FP6 project UERRA (http://www.uerra.eu) and the Copernicus Climate Change Service, and the data providers in the ECA&D project (https://www.ecad.eu). The study was supported by the HUMDROUGHT project funded by the National Science Centre (contract 2018/30/Q/ST10/00654).

References

Gringorten, I.I. (1963), A plotting rule for extreme probability paper, *J. Geophys. Res.* **68**, 3, 813–814, DOI: 10.1029/JZ068i003p00813.

McKee, T.B., N.J. Doesken, and J. Kleist (1993), The relationship of drought frequency and duration to time scales. **In:** *Proc. 8th Conf. on Applied Climatology, 17–22 January 1993, Anaheim, USA*, 179–184.

Wang, W., J. Wang, and R. Romanowicz (2021), Uncertainty in SPI calculation and its impact on drought assessment in different climate regions over China, *J. Hydrometeorol*. **22**, 6, 1369–1383, DOI: 10.1175/JHM-D-20-0256.1.

Received 17 November 2022
Accepted 20 December 2022

Publications of the Institute of Geophysics, Polish Academy of Sciences
Geophysical Data Bases, Processing and Instrumentation
vol. 443 (E-13), 2022, pp. 65–69
DOI: 10.25171/InstGeoph_PAS_Publs-2022-045
International Symposium on Drought and Climate Change, 24–25 November 2022

Climate Change and Karst Aquifers – Methodologies Review

Jelena KRSTAJIC[1,5,✉], Quanyi YE[2,5], Jennie STEYAERT[3,5], and Amin SHAKYA[4,5]

[1]University of Belgrade, Faculty of Mining and Geology, Department of Hydrogeology, Belgrade, Serbia

[2]University of New South Wales, Sydney, Australia

[3]Utrecht University, Department of Physical Geography, Utrecht, Netherlands

[4]Indian Institute of Science, Interdisciplinary Centre for Water Research, Bangalore, India

[5]Groundwater Youth Network, UNESCO

✉ krstajicj@yahoo.com

A b s t r a c t

Groundwater resources in many regions are not immune to climate change. More attention is being paid to the role of groundwater in maintaining ecological flows in rivers during a drought due to decreased precipitation and snowmelt under climate change. Karst aquifers are vulnerable to the increasing occurrence of climate extremes events. This abstract will give an overview of some modern approaches which are used in the assessment of the climate change impact on the karst groundwater. Methods include GIS implementation and remote sensing tools which can contribute to local, regional, and global scale research. Combining the modern research tools with traditional, in-situ obtained data, can lead to more reliable results and more sustainable water management in the future.

Keywords: climate change, GIS, karst, aquifer, remote sensing.

1. INTRODUCTION

Karst aquifers cover 15.2% of the global ice-free continental land (Goldscheider et al. 2020; World Karst Aquifer Map (WoKAM)). The largest percentage of them can be found in Europe (21.8%), while the largest absolute area all around the world is in Asia (8.35 million km²) (Stevanović et al. 2021). Karst aquifers around the world act as a partial source providing drinking

water for almost a quarter of the world's population (Ford and Williams 2007). Karst aquifers store considerable amount of water because it is composed of high-porosity carbonate rocks, which are usually more reactive on frequency of flooding and droughts resulting from climate change. Therefore, to quantify and mitigate the influence of changing, it is important to understand the aquifer characterisation and geological properties and assess aquifers' intrinsic features. In that way it is possible to develop a relevant approach in solving problems related to the aquifers' variable recharge, reservoirs, and drainage dynamics. It is the heterogeneity of the karst aquifers which leads to their different hydraulic behaviour during recharge periods. Karst aquifers might be a fast responder to rainfalls, but also can act as a "sponge" which can absorb a huge amount of water and only then start to drain it slowly.

Anticipating changes in climate and assessing their impact on karst aquifers is one of the most important tasks in securing safe water supply in the future. Therefore, much research in the past two decades was focused on the impact of climate changes on groundwater in different types of aquifers (Taniguchi and Holman 2010; Treidel et al. 2012; Stevanović et al. 2012). Hereby, the overview of some valuable methods for assessing of the climate change impact on karst aquifers will be presented. The aim of this extended abstract is to discuss the advantages of modern approaches in assessing the impact of climate change in the karst environment. In the following chapter, the Geological Information System (GIS) methods including Climate Changes Permeability and Storativity (CC PESTO), GALDIT, and Gravity Recovery and Climate Experiment (GRACE) approaches will be presented.

2. OVERVIEW OF THE GIS BASED METHODOLOGIES

2.1 CC PESTO method

One of the more recent methods, which was designed directly in the function of assessing the sensitivity of aquifers to climate change, is the CC PESTO method (Climate Changes – CC, PErmeability and STOrativity; Stevanović et al. 2021). This method aims to assess and map the vulnerability of karst aquifers to climate change. CC PESTO was tested on a karst aquifer due to the global importance of these waters, but also the complexity that karst terrains bring with them (Stevanović et al. 2021). This method evaluates intrinsic vulnerabilities without considering the human intervention. To achieve this, the aquifer conductivity, storage capacity and discharge regime are considered, as well as the slope of the terrain. This method requires the digitization of existing geological and hydrogeological maps, preparation of each parameter separately in the form of digital base maps. To achieve this, the conductivity, storage capacity and discharge regime are considered, as well as the slope of the terrain, where the slope is obtained via Digital Elevation Model (DEM). According to a specially defined algorithm, the weighting factors of all mentioned parameters are combined and as a result, the intrinsic vulnerability of the aquifer is visually presented.

This method provides valuable karst aquifer management information on protecting the aquifer from extreme climate events and contributes to the karst aquifer water management plan. Stevanović et al. (2021) emphasize that CC PESTO is flexible and applicable to all forms of karst landscape, but that it is necessary to determine the weighting factors for each parameter depending on the local conditions of the terrain on which it is applied.

2.2 GALDIT method

The sensitivity of groundwater to seawater intrusion can be defined as the sensitivity of groundwater quality to artificial extraction, or to sea level rise, or both when it comes to coastal areas. This sensitivity is determined by the characteristics of the aquifer. Seawater intrusion is one of the most common mechanisms of salinization that affect the quality of coastal aquifers. It is an

active process that leads to the disruption of the hydrodynamic equilibrium between fresh and sea water. One of the reasons for the occurrence of salinization is over pumping due to the constantly growing population in coastal areas, but also due to natural changes in feeding or raising the level of the world sea (Kouz et al. 2018). The GALDIT method for assessing the vulnerability of groundwaters to climate change was developed specifically for coastal areas and the assessment of seawater intrusion.

Principles of applying the GALDIT approach according to Kouz et al. (2018) is based on a classification system and is a qualitative method based on six parameters:

(G – Groundwater Occurrence) Occurrence of groundwater, and as part of that, vulnerability to marine intrusion is considered in relation to the type of aquifer, which can be closed, semi-closed and open, where the open aquifers will be the most exposed to seawater intrusion;

(A – Aquifer Hydraulic Conductivity) For the same pumping capacity (or natural flow), the acceleration of the contact of fresh and salt water is closely related to the hydraulic conductivity;

(L – Height of Groundwater Level below Sea Level) This parameter determines the hydraulic pressure that allows pushing the contact of fresh and salt water. Groundwater level in correlation to mean sea level is a very important factor in controlling the progress of saltwater intrusion and assessing marine intrusion into the coastal aquifer;

(D – Distance from the Shore) The distance from the shore is measured perpendicular to the shore. The impact of saltwater intrusion decreases with distance from the coast;

(I – Impact of existing status of seawater intrusion in the area) Parameter is represented in the spatial variation of the ratio – $Cl^-/HCO_3^- + CO_3$. Chloride is the dominant anion in seawater, while it is very little present in fresh water;

(T – Thickness of the aquifer) The greater the volume of the aquifer is, the greater is the importance of the extension of saltwater intrusion.

By combining all maps obtained (for each described factor), using the appropriate algorithms, the final vulnerability map will be produced. Overlapping of parameter maps (basemaps) is similar procedure as it was for CC PESTO method. This approach is commonly known for the GIS based groundwater vulnerability mapping.

3. GRACE SATELITES DATA APPROACH

Special attention should be given to satellite technology and the launch of the GRACE (Gravity Recovery and Climate Experiment) satellite in 2002. The main difference between the previous uses of satellite research and remote sensing in general and GRACE tools is that other satellite analyses of water resources are based on radiometric measurements of the Earth's surface, while GRACE provides data based on changes in gravity (Swenson and Famiglietti 2012). Hydrological resolution of GRACE is debated, depending on the required accuracy of estimate and it is coarse in general. These changes in time occur mainly due to the redistribution of mass within the Earth's fluid layer, on a daily to decadal scale. The cause can be found in tectonic movements or glacial isostatic signals, but also in changes in surface concentrations in the atmosphere, oceans and continental water bodies (Leblanc et al. 2012). From its launch until today, the GRACE satellite has been used to assess changes in terrestrial water reserves, with increasing use in assessing changes in groundwater reserves.

4. DISCUSSION AND CONCLUSION

The underlying principle of discussed GIS based methods are similar. These methods require digitization, vectorization and rasterization of data in GIS, apply algorithms proposed and obtain the final vulnerability map. Vulnerability classes are also similarly ranked in the final vulnerability maps. Difference in each method is observed in the number of parameters that are included in the final algorithm for obtaining the vulnerability map. Furthermore, GALDIT method includes the observed intrinsic vulnerability to seawater intrusion, which indirectly introduces a qualitative parameter as one of the participants in the groundwater vulnerability assessment, while CC PESTO method is oriented towards the quantitative sensitivities of karst groundwater. When it comes to GRACE satellite data it is concluded that its application is the most successful when it comes to global and regional assessments of the groundwater reservoir change. For applying this method on local scales, the special data downscaling shall be done. It is recommended that, whenever possible, results obtained by this method are calibrated by the traditional, field work based approaches and calculations.

Ultimately, it is obvious that these methods might be a powerful tool in assessing climate change impact on karst aquifers if handled carefully by groundwater experts.

References

Ford, D., and P. Williams (2007), Karst water resources management. **In:** D. Ford and P. Williams, *Karst Hydrogeology and Geomorphology*, John Wiley & Sons Ltd., 441–469.

Goldscheider, N., Z. Chen, A.S. Auler, M. Bakalowicz, S. Broda, D. Drew, J. Hartmann, G. Jiang, N. Moosdorf, Z. Stevanović, and G. Veni (2020), Global distribution of carbonate rocks and karst water resources, *Hydrogeol. J.* **28**, 5, 1661–1677, DOI: 10.1007/s10040-020-02139-5.

Kouz, T., H. Cherkaoui Dekkaki, S. Mansour, M. Hassani Zerrouk, and T. Mourabite (2018), Application of GALDIT index to assess the intrinsic vulnerability of coastal aquifer to seawater intrusion: Case of the Ghiss-Nekor aquifer (North East of Morocco). **In:** M.L. Calvache, C. Duque, and D. Pulido-Velazquez (eds.), *Groundwater and Global Change in the Western Mediterranean Area*, Environmental Earth Sciences, Springer International Publishing AG, 169–178.

Leblanc, M., S. Tweed, G. Ramillien, P. Tregoning, F. Frappart, A. Fakes, and I. Cartwright (2012), Groundwater change in the Murray basin from long-term in-situ monitoring and GRACE estimates. **In:** H. Treidel, J.L. Martin-Bordes, and J.J. Gurdak (eds.), *Climate Change Effects on Groundwater Resources – A Global Synthesis of Findings and Recommendations*, CRC Press, Boca Raton, 169–190.

Stevanović, Z., V. Ristić, and S. Milanović (2012), *CC WATERS Climate Changes and Impact on Water Supply*, University of Belgrade, Faculty of Mining and Geology, Department of Hydrogeology, Belgrade, Serbia.

Stevanović, Z., V. Marinović, and J. Krstajić (2021), CC-PESTO: a novel GIS-based method for assessing the vulnerability of karst groundwater resources to the effects of climate change, *Hydrogeol. J*. **29**, 159–178, DOI: 10.1007/s10040-020-02251-6.

Swenson, S., and J. Famiglietti (2012), Sustainable groundwater management for large aquifer systems: tracking depletion rates from space. **In:** H. Treidel, J.L. Martin-Bordes, and J.J. Gurdak (eds.), *Climate Change Effects on Groundwater Resources – A Global Synthesis of Findings and Recommendations*, CRC Press, Boca Raton, 367–376.

Taniguchi, M. (2012), Grounwater management in Asian cities under the pressures of human impacts and climate change. **In:** H. Treidel, J.L. Martin-Bordes, and J.J. Gurdak (eds.), *Climate Change Effects on Groundwater Resources – A Global Synthesis of Findings and Recommendations*, CRC Press, Boca Raton, 341–350.

Taniguchi, M., and I.P. Holman (eds.) (2010), *Groundwater Response to Changing Climate*, International Association of Hydrogeologists Selected Papers, Vol. 16, CRC Press, Boca Raton.

Treidel, H., J.L. Martin-Bordes, and J.J. Gurdak (eds.) (2012), *Climate Change Effects on Groundwater Resources – A Global Synthesis of Findings and Recommendations*, International Association of Hydrogeologists, CRC Press, Boca Raton.

Received 17 November 2022
Accepted 20 December 2022

"Publications of the Institute of Geophysics, Polish Academy of Sciences: Geophysical Data Bases, Processing and Instrumentation" appears in the following series:

A – Physics of the Earth's Interior

B – Seismology

C – Geomagnetism

D – Physics of the Atmosphere

E – Hydrology (formerly Water Resources)

P – Polar Research

M – Miscellanea

Every volume has two numbers: the first one is the consecutive number of the journal and the second one (in brackets) is the current number in the series.